

CITIZENSHIP C 308398

AS

RESEARCH ON
MICROWAVE WINDOW MULTIPACTOR
AND ITS INHIBITION

REPORT NUMBER 2

CONTRACT NUMBER DA 36-039-SC-90818
DEPARTMENT OF THE ARMY
TASK NUMBER OST 76-10-318-28-03

SECOND QUARTERLY PROGRESS REPORT
1 October 1962 through 31 December 1962

U. S. ARMY ELECTRONICS RESEARCH AND DEVELOPMENT LABORATORY
FORT MONMOUTH, NEW JERSEY

EITEL-McCULLOUGH, INC.
San Carlos, California

408 398

NO. 015

Qualified requestors may obtain copies of this report from the Armed Services Technical Information Agency (ASTIA), Arlington Hall Station, Arlington 12, Virginia. ASTIA release to OTS is not authorized.

RESEARCH ON
MICROWAVE WINDOW MULTIPACTOR
AND ITS INHIBITION

REPORT NUMBER 2

CONTRACT NUMBER DA 36-039-SC-90818
DEPARTMENT OF THE ARMY
TASK NUMBER OST 76-10-318-28-03

SECOND QUARTERLY PROGRESS REPORT
1 October 1962 through 31 December 1962

U. S. ARMY ELECTRONICS RESEARCH AND DEVELOPMENT LABORATORY
FORT MONMOUTH, NEW JERSEY

EITEL-McCULLOUGH, INC.
San Carlos, California

RESEARCH ON
MICROWAVE WINDOW MULTIPACTOR
AND ITS INHIBITION

REPORT NUMBER 2

CONTRACT NUMBER DA 36-039-SC-90818
DEPARTMENT OF THE ARMY
TASK NUMBER OST 76-10-318-28-03

SECOND QUARTERLY PROGRESS REPORT
1 October 1962 through 31 December 1962

Object of Research: (1) Attain a more complete theoretical understanding of microwave tube window multipactor, its inhibition and sustainment, and the tube performance limitations it imposes; (2) Investigate techniques to inhibit multipactor without degrading tube performance.

Prepared by: Oskar Heil
Oskar Heil

Donald Preist
Donald Preist

This research is a part of Project DEFENDER, sponsored by the Advanced Research Projects Agency, Department of Defense, under ARPA Order Number 318-62, Project Code Number 7300, and is conducted under the technical guidance of the U. S. Army Electronics Research and Development Laboratory, Fort Monmouth, New Jersey.

Qualified requestors may obtain copies of this report from the Armed Services Technical Information Agency (ASTIA), Arlington Hall Station, Arlington 12, Virginia. ASTIA release to OTS is not authorized.

TABLE OF CONTENTS

<u>Section</u>		<u>Page</u>
1	Purpose	1
2	Abstract	2
3	Publications, Lectures, Reports and Conferences	4
4	Task A	5
	4.1 Factual Data - Progress to Date	6
	4.2 Conclusions	32
	4.3 Program for Next Interval	33
5	Task B	36
	5.1 Factual Data - Progress to Date	37
	5.2 Conclusions	64
	5.3 Program for Next Interval	65
6	Identification of Key Technical Personnel	66

1. PURPOSE

The broad purpose of the study is to provide a deeper understanding of multipactor effects at waveguide windows used with high power microwave tubes which will lead to practical methods for preventing or eliminating multipactor, thereby raising the power handling capacity of windows. Throughout the investigation emphasis will be placed on a scientific approach and understanding of the phenomena involved so that solutions may be obtained in the most general terms and can therefore be expected to be applicable over a wide range of conditions.

At present, the method of eliminating multipactors is the application of an evaporated film of titanium in order to reduce the secondary emission coefficient of the window and adjacent surfaces, using techniques which have already been developed to a certain point as a result of the company-sponsored research at Eitel-McCullough on cylindrical windows prior to the inception of the present contract. This work has been summarized in two published articles¹. In the course of this work klystrons were made with coated output windows and adjacent metal parts. Those windows without coatings exhibited severe multipactor, and with coatings exhibited no multipactor. At the time of the inception of the contract it had not been done anywhere else, to our knowledge. It seems reasonable to suppose that these techniques would be equally effective if applied to waveguide windows at which multipactor discharges are occurring. Another possible method would be that originally proposed by O. Heil in 1960, which is the direct application of titanium suboxides, rather than titanium metal.

An alternate method of eliminating multipactor is provided by phase or space defocusing of the electron cloud near the window. If the electric fields in the window region are properly shaped, or if the window configuration is suitably designed, the secondary electrons produced will not be entrapped in a resonant field. This method does not, in principle, require a reduced secondary emission coefficient at the window surface. However, these two approaches are mutually beneficial, and together should provide a very effective means of suppressing multipactor.

¹"On the Heating of Output Windows of Microwave Tubes by Electron Bombardment," by D. H. Preist and R. C. Talcott, IRE Trans. PGED Vol. ED-8 No. 4, July 1961, and "The Effects of Titanium Films on Secondary Electron Emission Phenomena in Resonant Cavities and at Dielectric Surfaces," by R. C. Talcott, IRE Trans. on Electron Devices, Vol. ED-9, No. 5, Sept. 1962, pp 405-410.

Because these approaches are quite different in application, the work has been divided into the following two tasks, with separate investigators:

TASK A: An Experimental Study of Electron Bombardment Phenomena at the Output RF Windows of High Power Microwave Tubes.

Phase 1. Experimental and analytical study of multipactor effects at waveguide windows under high power conditions.

Phase 2. Development and application of evaporation coatings and techniques applied to the window and surrounding metal parts in order to reduce secondary emission coefficient to less than unity.

TASK B: Study of the Inner-Window Surface and Configurations Affecting Power Handling Capabilities of High Power Microwave Tubes.

Phase 1. Analysis of various means of obtaining space and phase defocusing of electrons by shaping the fields and window surfaces.

Phase 2. Study of materials and coatings in conjunction with shaped fields to develop windows capable of handling higher powers without multipactor.

2. ABSTRACT

TASK A: An Experimental Study of Electron Bombardment Phenomena at the Output of RF Windows of High Power Microwave Tubes

This second quarterly report on the study and elimination of multipactor discharges at waveguide windows of high power microwave tubes reports progress on the two major phases, which are:

1. An analytical and experimental study of multipactor effects at waveguide windows using a frequency of 2850 megacycles under both CW and pulsed conditions, and
2. The development and application of evaporative coatings and techniques to waveguide windows and the testing of these coated windows under

multipactor conditions to evaluate the effects of the coatings in preventing multipactor.

Phase 1. CW and pulse tests on round disc windows at 2850 megacycles have shown that a multipactor discharge, believed to be the single surface type, exists when the electric field strength exceeds a certain value. This value appears to be the value predicted by the theory previously developed during research on cylindrical windows at 650 megacycles. Magnetic fields have been used to encourage the multipactor but four (4) windows tested showed multipactor without the magnetic fields. Both beryllia and alumina windows exhibit the multipactor, which may occur when the equivalent transmitted power is about 135 kilowatts or higher. So far no coated windows have been tested, and the tests have been limited to about 2 megawatts equivalent transmitted power.

Phase 2. A new method of controlling evaporative coatings on disc windows has been thought of, because the method outlined in the first quarterly report has not come up to expectations. During the next period, tests will be made at higher power levels and coated windows will be tested.

TASK B: Study of the Inner Window Surface and Configurations Affecting Power Handling Capabilities of High Power Microwave Tubes

In this quarter some of the ideas described in the first quarterly report concerning grooved window surfaces and titanium suboxide coatings were tested in the Stanford linear accelerator ring resonator. Results of the tests showed that the multipactor is completely eliminated on Al 300 windows by grooving the face and coating the crests of the grooves. Also, it is eliminated by coating ungrooved windows in a dotted pattern. By grooving the surface of silica windows without any coating, the multipactor is eliminated and these windows withstand 87 megawatts peak at 15 kw average power and 40 megawatt peak at 40 kv average without any damage. These

were the power limits of the ring resonator so the tests could not be run at greater power levels.

Failures on flat alumina windows by puncturing are discussed. It is shown that the gliding multipactor is favored by a small angle between the window surface and the direction of the electric h.f. field because of a favorable phasing effect in the release of secondary electrons. This effect is observed experimentally. The radiation pressure on electrons is described as another effect giving electrons a dc velocity which can be big enough to cause an appreciable difference for the formation of the multipactor on the input or the output side of windows.

3. PUBLICATIONS, LECTURES, REPORTS AND CONFERENCES

3.1 Conferences Held

3.1.1 At Eitel-McCullough, San Carlos, California, with Mr. Louis Heynick of the U. S. Army Electronics Research and Development Laboratory, October 5 and October 8, 1962.

Plans and progress were reviewed.

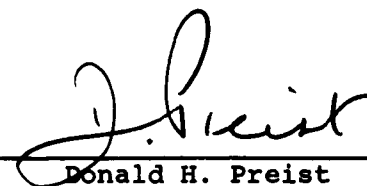
3.1.2 At Eitel-McCullough, San Carlos, California, with Lt. Col. W. B. Lindsay of ARPA and Mr. Louis Heynick of the U. S. Army Electronics Research and Development Laboratory, November 29, 1962.

Plans and progress were reviewed.

4. TASK A

AN EXPERIMENTAL STUDY OF ELECTRON BOMBARDMENT PHENOMENA
AT THE OUTPUT RF WINDOWS OF HIGH POWER MICROWAVE TUBES.

Prepared by:


Donald H. Preist

4. TASK A

4.1 FACTUAL DATA - PROGRESS TO DATE

4.1.1 Tests of Windows

Four test units of the design described in the first quarterly report were built and tested. Results were satisfactory except that the coupling iris was too small in the first units. This was remedied. Also, some difficulty has been experienced in obtaining a good rf compression seal. A drawing of the window box is shown in Figure 1.

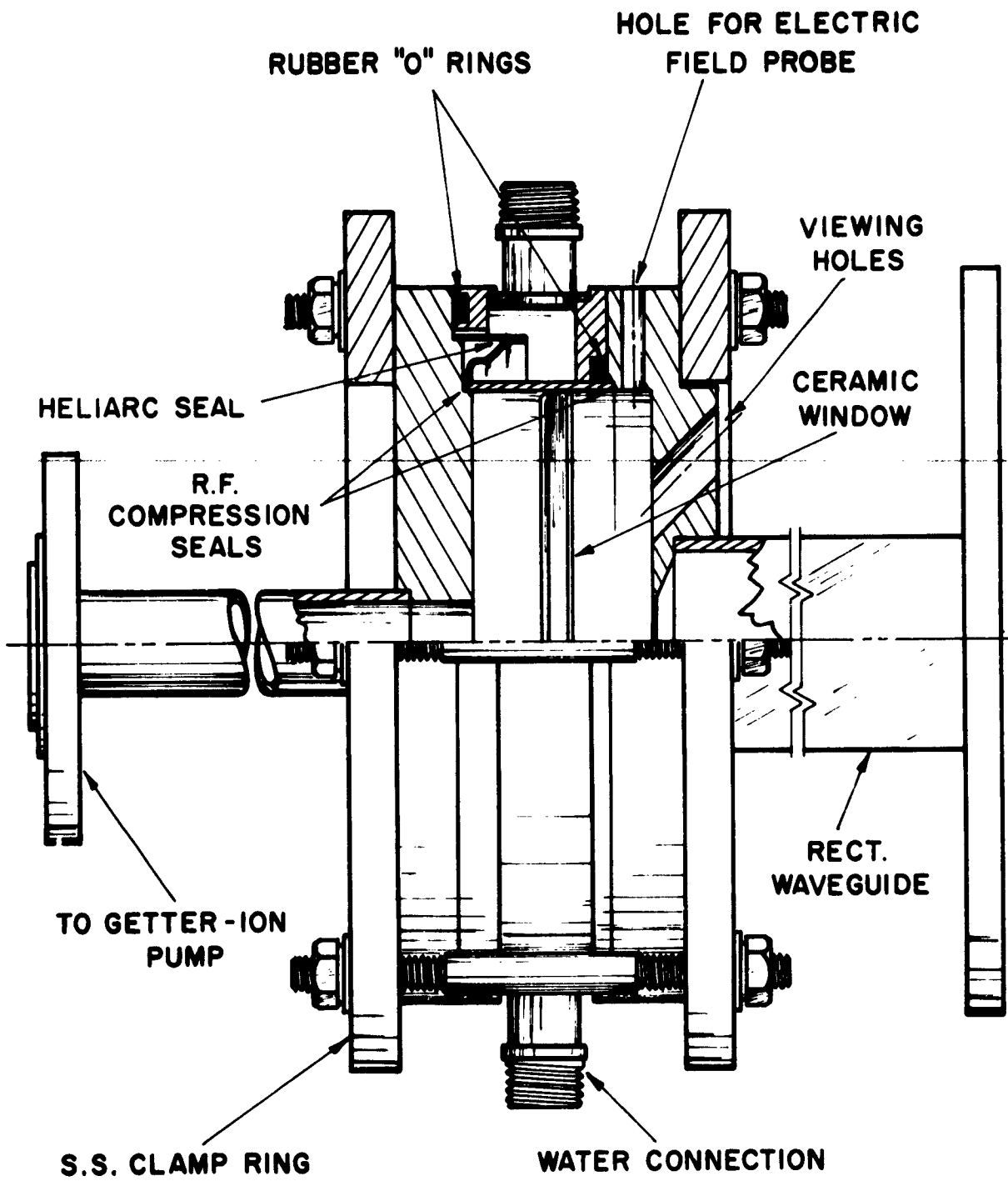
~~The klystron rf generator was set up, tested, and equipped with a pulser which allowed a wide range of pulse lengths and duty cycles to be obtained from it.~~

Also, an electromagnet was made so that a static magnetic field could be applied to the window box in either of two directions - one direction being parallel to the electric field and the other making the two fields perpendicular and mutually perpendicular to the axis of the cavity. It was anticipated that this magnet would throw more light on the behavior of the window under multipactor conditions and could be used to induce multipactor in some cases. This was borne out by the results, as will be seen. All tests were performed at 2850 ± 15 Mc and all windows were uncoated and baked out at 500°C for 4 hours on a standard oil diffusion vacuum pump system equipped with refrigerated baffle and liquid nitrogen trap.

All windows, when assembled into the window box, were checked on a cold test set-up for VSWR, resonant frequency, and Q before and after hot testing.

4.1.1.1 First Window Tested (Coors BD96 BeO)

First, CW power was fed into the window box. The power level was raised and the power dissipated was measured by two methods: firstly, by using the directional couplers in the waveguide run to the window box and, secondly, by measuring the power



"WINDOW BOX" ASSEMBLY

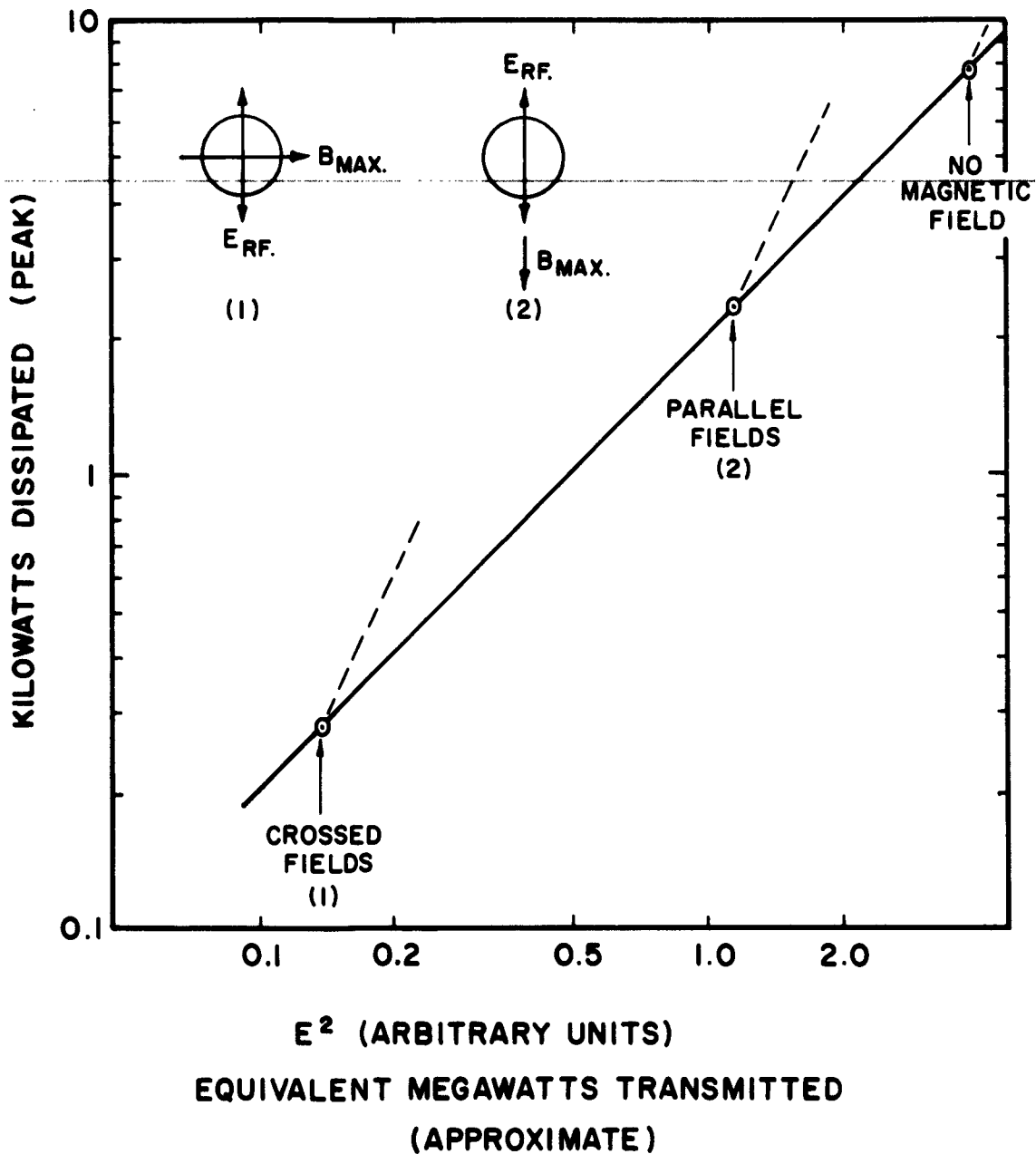
appearing in the water cooling jackets around the window box. After calibration of the directional couplers, these two power dissipation measurements agreed within a few per cent. Without using magnets the power was taken up to the point where more than 900 watts was being dissipated in the window. The test was stopped here for fear of cracking the window if more power was applied. The plot of power dissipation against electric field squared (the electric field being measured with a bolometer connected to the probe adjacent to the window) showed a linear relationship indicating no multipactor. The rf driver was then pulsed and the power level was raised further, until about 10 KW peak power and a few hundred watts average power were dissipated in the window box. At about this level the plot showed the beginning of a multipactor. This can be seen in Figure 2.

We could not increase the power level because of the limitation of the klystron power supply. Next the magnet was turned on with the magnetic and electric fields parallel. The magnet was strong enough to allow, for short periods, field strengths up to 1.5 x the cyclotron resonance field strength B_c at the frequency used. The field was continuously variable. When running the windows at less than the peak power previously used it was immediately obvious that the magnets were increasing the power dissipated. Next we determined the minimum electric field strength above which the magnet would have any effect at all for any value of field. This was quite well defined and is also indicated on Figure 2. Next the magnet was rotated so that the electric and magnetic fields were crossed. It was then found that the magnets would have an effect at even lower magnetic field strengths and again the minimum electric field strength above which the magnet would have an effect was carefully measured and is shown on Figure 2.

Also, the power dissipation versus electric field strength squared was plotted for constant values of magnetic field with results shown in Figure 3.

WINDOW N° TU-1 (BeO)

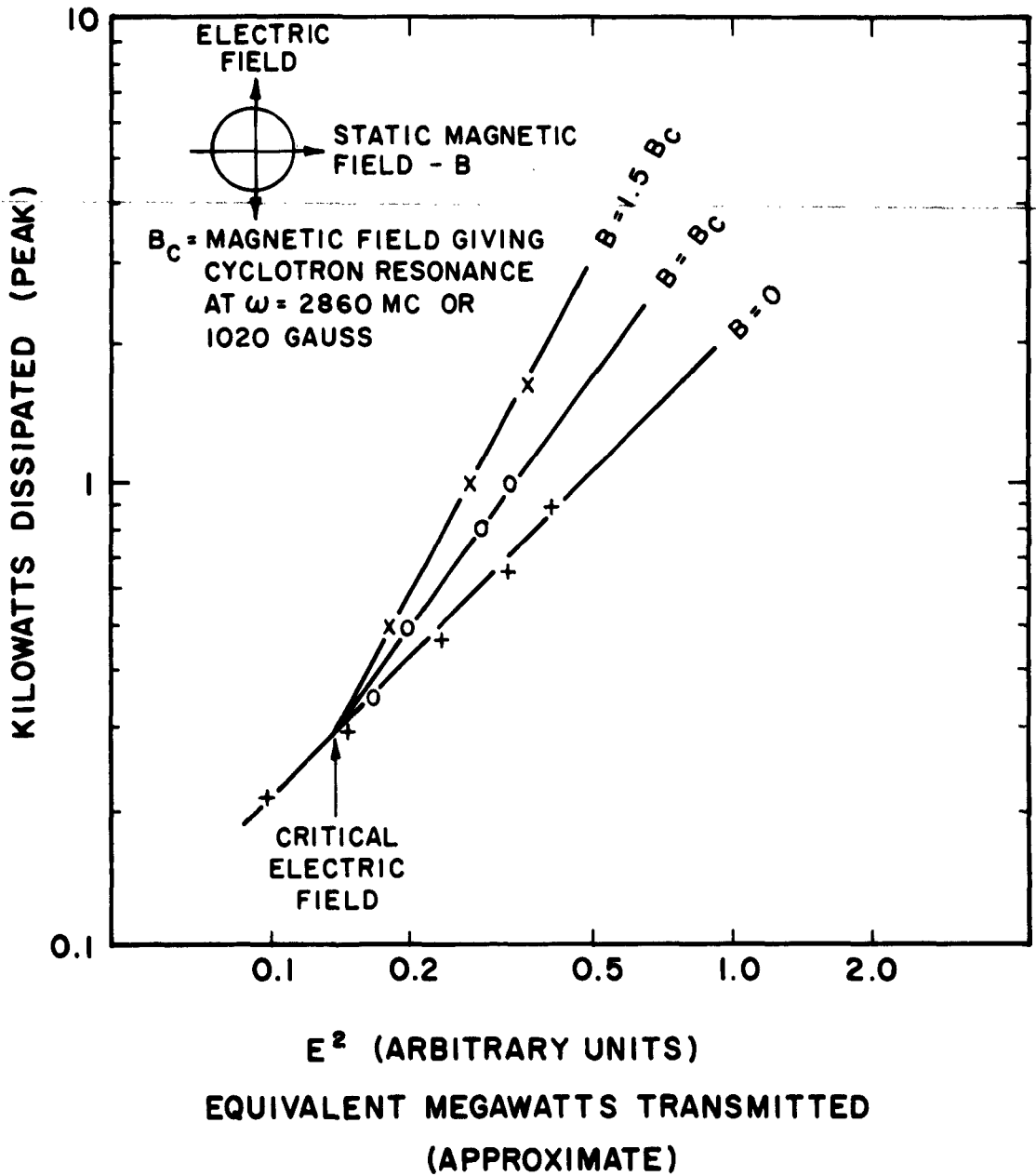
THRESHOLD POWER LEVELS FOR WINDOW
MULTIFACTOR WITH AND WITHOUT STATIC
MAGNETIC FIELD. $F = 2860$ MC



WINDOW N^o TU-1 (BeO)

WINDOW MULTIPACTOR WITH CROSSED
FIELDS OF DIFFERENT VALUES

F = 2860 MC



During all these measurements notes were taken of the apparent vacuum or gas pressure as measured by the vac-ion pump gauge attached to the window box. Whenever it was found that the magnet would affect the situation it was noted that the vac-ion gauge indicated a higher residual pressure. The residual pressure without power applied to the window box is on the order of 2 to 5×10^{-9} Torr. Under conditions of strong multipactor the pressure would rise as high as 10^{-5} Torr.

All the effects measured were reversible and there was no hysteresis. Finally, the window was let down to air and, again, power dissipated was measured as a function of e^2 and the resulting plot showed complete linearity. The magnets had no effect.

4.1.1.2 Window No. 2 (Wesgo AL995 Alumina)

This window of alumina was tested in the same way as Window No. 1. It was found that non-linearity occurred without the use of the magnets at a much lower power level than the Window No. 1. The result is shown in Figure 4.

4.1.1.3 Window No. 3 (Coors BD96 BeO)

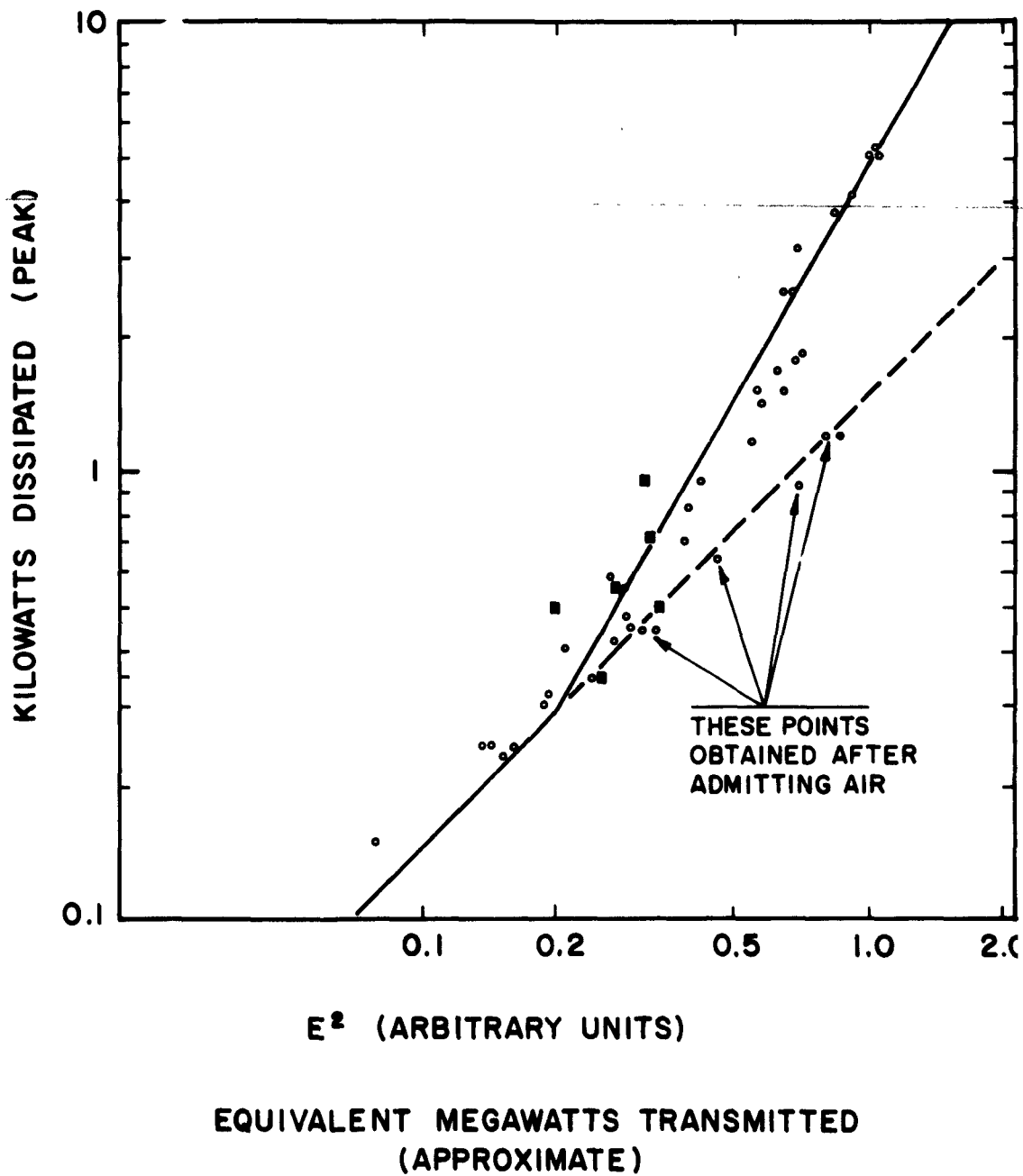
This window was tested with very erratic results, subsequently found to be due to a malfunction of the rf generator. During the tests it was clear that the magnetic field was affecting the performance as with the other windows. After the equipment had been fixed the window behaved linearly. Examination showed that the window had developed a leak and had gone down to air in the meantime.

4.1.1.4 Window No. 4 (Coors BD96 BeO)

The results of the tests on this window are shown in Figure 5. The equipment had been improved somewhat and was more stable. Also, the matching iris had been more carefully adjusted and measurements were more accurate. The figure shows the result without magnets and also with the crossed magnetic field. It was observed on this window and also on Nos. 2 and 3 that at the higher power levels a small

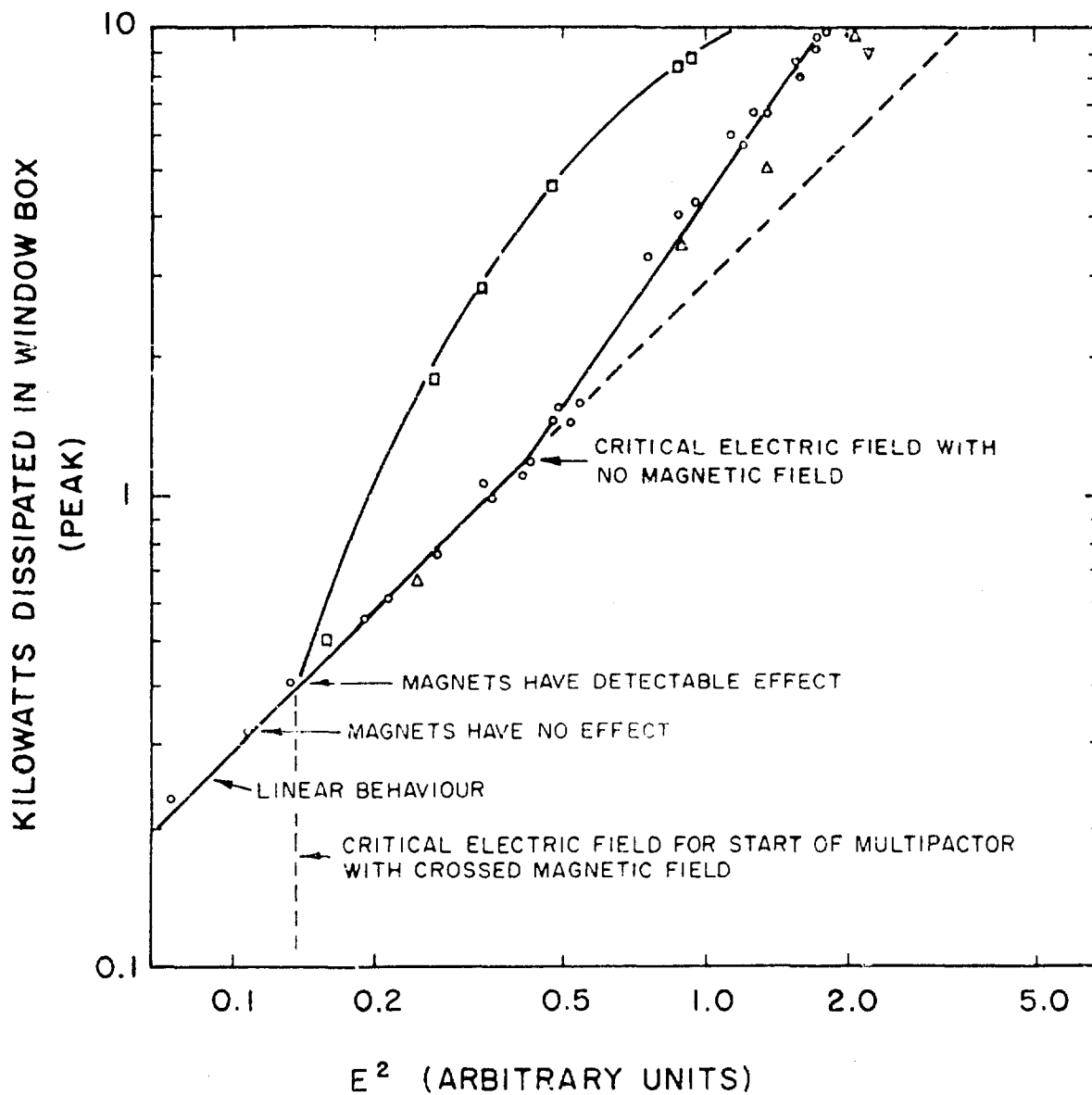
WINDOW N^o TU-2 (Al₂O₃)

■ - POINTS OBTAINED WITH MAGNETS
○ - POINTS OBTAINED WITHOUT MAGNETS



WINDOW N° TU-4 (BeO)

- - NO MAGNETIC FIELD
- - POINTS WITH CROSSED MAGNETIC FIELD HAVING VALUE $1.2 B_c$
- △ - " " " $0.4 B_c$
- ▽ - " " " $0.2 B_c$



EQUIVALENT MEGAWATTS TRANSMITTED (APPROXIMATE)

crossed magnetic field would decrease the dissipation for given transmitted power. These points are shown on the figure.

During non-linear behavior, close examination of the leading edge of the rf pulse was made to see if the delay in starting of the non-linear loading was measurable. It was not. Also, the duty cycle was varied between 1/500 and unity without effect on the plot of window dissipation versus electric field strength squared.

4.1.2 Analysis of Test Results

The main conclusion to be drawn from these tests is that some sort of multipactor discharge is, in fact, occurring at all the windows above a certain power level. The proofs that the discharge is an electron discharge are that the characteristics are affected by magnetic fields and that there is no non-linear behavior when air is admitted to the cavity. It should be remembered that all the windows tested were uncoated. Regarding the type of multipactor discharge, the strong resemblance between the curves of power dissipated versus field strength at the window squared to the results previously obtained with cylindrical windows are strongly suggestive that the same type of multipactor is occurring in both cases. In the case of the cylindrical window a fairly exhaustive series of tests and analysis had shown clearly that the effect was a single surface one⁽¹⁾. The possibility of two surface multipactors between the window and the surrounding metal has been considered, and seems unlikely, although plans are being made to look for this more closely during the next quarter.

We shall assume, for the moment, that the multipactor observed is, in fact, the single surface variety. A mathematical treatment of the conditions necessary to start it is given in para. 4.1.3. We would expect to observe the following:

1. As power level is raised, the discharge should begin at the center of the window,

where the electric field strength is highest, and should then spread to the other parts.

2. The critical electric field strength required to start the discharge should be that which gives secondary electrons accelerated for half an rf cycle enough energy to release more than one new secondary on impact at the window. The electric field, the frequency, and the energy are related by the following equation:

$$V_1 = \frac{2e}{m} \left(\frac{E_{rf}}{\omega} \right)^2 + V_0 \quad (1)$$

Where V_1 is the kinetic energy in volts

Where V_0 is initial velocity of emission, in volts

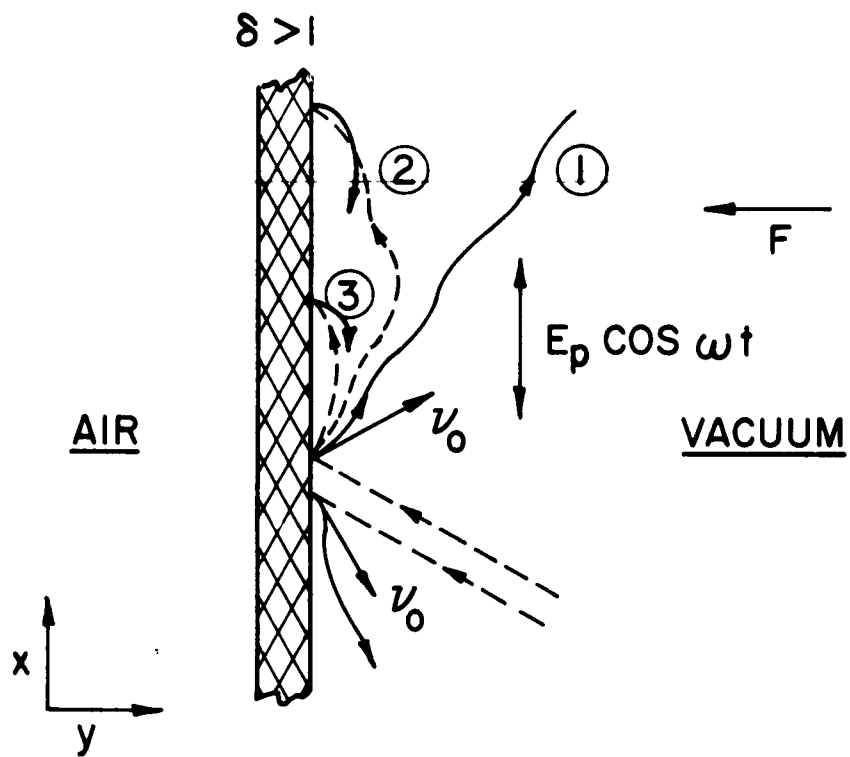
Where $\frac{e}{m}$ is the electron charge to mass ratio, taken as 1.76×10^{11}

Where E_{rf} is the peak value of electric field strength in volts per meter

Where ω is the rf angular frequency in radians per second

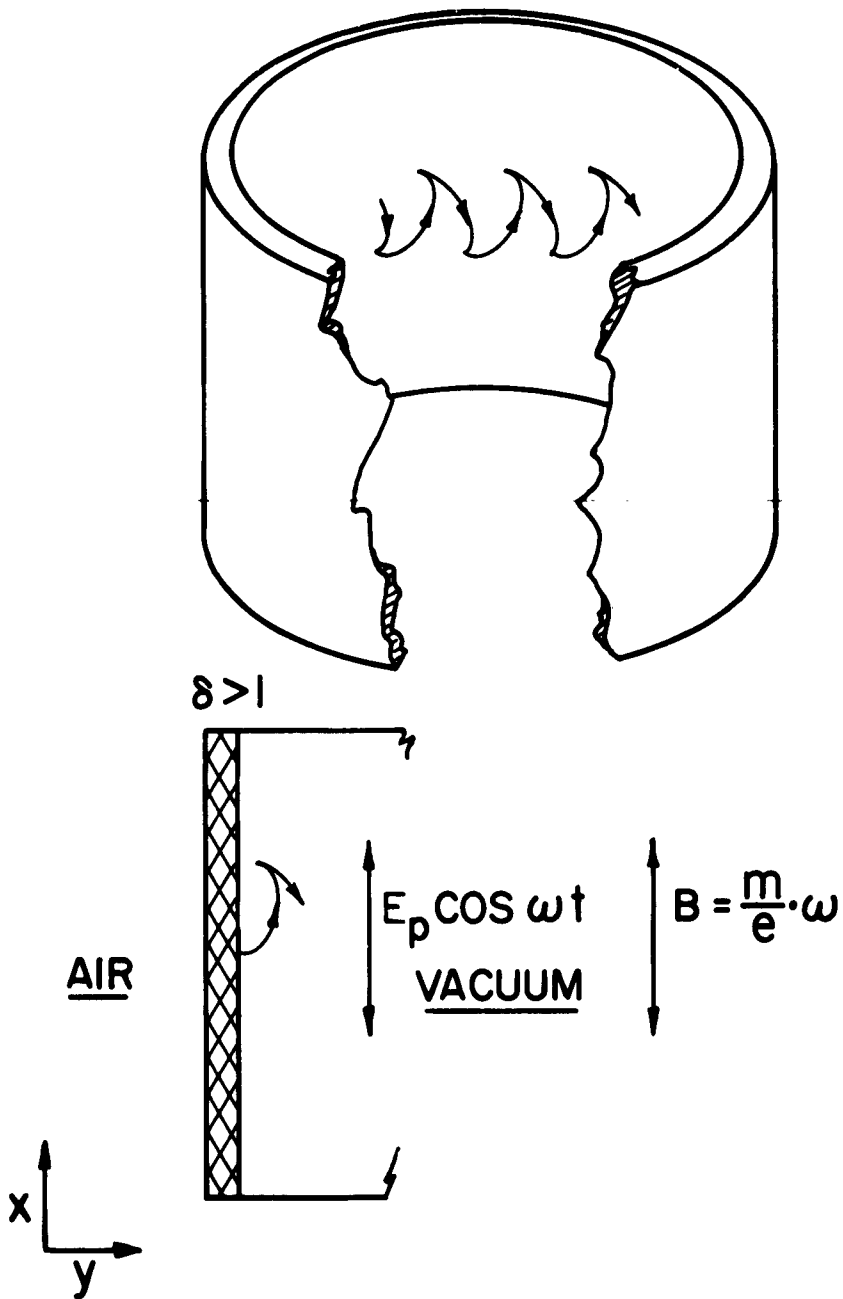
It should be noted that the critical field strength given by this expression is linearly proportional to frequency, for a given value of V_1 .

3. The electron dynamics are illustrated in Figure 6 for no magnetic field, and in Figure 7 for parallel magnetic and electric fields having the values shown. A cylindrical window is shown in Figure 7 but the same situation will exist at a flat window. At the critical field strength, synchronism between the electron motion and the electric field is necessary and the time of flight of electrons must be $n\pi$ radians, where n is any integer. At higher field strengths, departure from synchronism is permitted.



ELECTRON MOTIONS WITH ZERO
MAGNETIC FIELD

- ① $F = 0$
- ② $F_1 > 0$
- ③ $F > F_1$



ELECTRON MOTIONS WITH AXIAL MAGNETIC
FIELD HAVING THE CYCLOTRON RESONANCE
VALUE

4. A restoring force, shown as F in Figure 6, is required to bring the electrons back to the surface, since they all leave with a finite component of velocity normal to the surface. This force may be provided by non-homogeneous rf electric fields as described by Heil in the first Quarterly Progress Report, if the field strength at the window is less than that at some adjacent plane. The force may also be provided by a static positive charge on the window surface, giving an electrostatic field, by magnetic forces if magnetic fields are used, or by field gradients caused by space charge produced by the multipactor itself.
5. Above the critical field, the power dissipated at the window will rise more rapidly than linearly with E^2 , the exact relationship presumably depending on several factors including space charge defocusing, variations in restoring force F, and the rate of net loss of electrons from the system.

Considering each of these characteristics in turn, in connection with the experimental observations, the following comments can be made:

Concerning (1)

The viewing holes did allow observation of a visible glow during multipactor, but the holes were not numerous enough to tell exactly where the multipactor started. The next window box design should allow this to be observed much more clearly on the vacuum surface.

Concerning (2)

It is of interest to see if the critical field strength measured agrees with the calculated field strength. The critical field is presumably the lowest field at which the multipactor can be induced to start by using magnetic fields, since the magnetic fields cannot produce linear

acceleration and cannot add to the electron kinetic energy with the field configurations used, and therefore, affects only the restoring force F . In the experiments, only the power dissipated at the window can be measured at the critical electric field strength. The value of the field must be calculated. Two methods of calculation, both approximate, have been used.

The first method uses two measured values of Q , one for the window box containing the window (Q_1), the other for the same window used as on a klystron, and terminated by a matched waveguide (Q_2). The ratio $\frac{Q_1}{Q_2}$ gives ratio of power transmitted to power dissipated in the window box, approximately only, since the coupling iris aperture is quite different in the two cases and the field at the window is not precisely the same. Also, the power dissipated in the window box is not only that lost in the window and the window seal, but also includes copper losses in the resonant cavity walls. These walls are different in the two cases because (a) the iris aperture is different and (b) the axial length of the cylindrical metal window mount is different.

Knowing the approximate power transmitted, it is possible to calculate the field strength if the ratio $\frac{E^2}{P_T}$ is known. This ratio is

known for an unperturbed circular waveguide. The presence of the window perturbs the guide to a degree dependent on the nature of the matching system. The type of window matching configuration commonly used, such as the pill box or type C window, will increase the field strength at the window above that in the guide but cannot decrease it. We can, therefore, say that the field strength at the window may be greater but cannot be less than the value given by Equation 2 for an unperturbed circular waveguide:

$$\frac{P_T}{E^2} = 1.99 \times 10^{-3} a^2 \frac{\lambda}{\lambda_g} \quad (2)$$

where P_T is equivalent transmitted power
in watts

where E is in v/cm

where a is radius in cm

where λ_g is guide wavelength

where λ is operating wavelength

The second method of arriving at the window field strength is to calculate the electric field distribution over the window surface, and then, knowing the loss factor of the ceramic used, and its volume, to calculate the total dielectric loss as a function of the maximum electric field strength.

Assuming that the losses in the seal and the copper losses in the window box are small by comparison with the dielectric loss in the ceramic, one may then use the measured total dissipation in conjunction with the above calculation to determine the maximum electric field at the window. This method is likely to be more accurate than method (1) because no assumptions have to be made about $\frac{E^2}{P_T}$. In calculating the

corresponding P_T however, the same assumption has to be made as with method (1).

The results of these two calculations for the beryllium oxide BD96 windows tested are as follows:

	$\frac{E_{\text{critical}}}{E_{\text{critical}}}$ (measured)	$\frac{E_{\text{critical}}}{E_{\text{critical}}}$ (calculated)	
	<u>Method 1</u>	<u>Method 2</u>	<u>Average of both Methods</u>
TU - 1	0.83	0.85	0.84
TU - 3	1.05	0.88±	0.97
TU - 4	1.18	0.99	1.08

Using Equation (1) and assuming $V_1 = 80$ v, gives $E_{\text{critical}} = 2700$ v/cm. In a matched unperturbed circular waveguide in the $TE_{1,1}$ mode 3.7" dia. this would correspond to a transmitted power of 135 KW. This agreement is probably as good as can be expected

bearing in mind the probable error in the calculation and the uncertainty in the actual value of bombarding voltage for beryllia ceramic which makes equal to unity. The scale on the abscissae of Figures 2 and 5 is adjusted to make the observed critical field correspond to a transmitted power of 135 KW.

We note that previous measurements and calculations made on windows under multipactor conditions at a much lower frequency (645 megacycles) also indicated that Eqn. 1 was substantially correct.⁽¹⁾ We therefore have some confirmation that the multipactor conditions were basically similar in the two cases and this lends some weight to the conclusion that this type of single surface multipactor is, in fact, occurring at the S-band windows under discussion here.

Concerning (4)

Since in the window box configurations used the dielectric field is stronger at the window than anywhere else, it is clear that all the field inhomogeneity forces are such as to accelerate electrons away from the window surface, and they cannot provide the restoring force F . The fact that the windows do multipactor must, therefore, be accounted for by some other restoring force which overcomes the forces due to the field inhomogeneities. It would appear that the only possible force is that due to a positive electrostatic charge on the window surface, as previously found in our earlier work on cylindrical windows.⁽¹⁾ Consideration of the electron dynamics suggests that such a positive charge is bound to exist, at least under multipactor conditions, because it can be shown that there is a net loss of electrons from the window surface. What is not completely clear is how the multipactor starts, because until the positive charge exists the multipactor cannot start and the positive charge will not exist until there is net loss of electrons from the window. Such a net loss may perhaps be explained by one or more of the following mechanisms:

- a. The arrival at the window of electrons from the surrounding environment having

sufficiently high velocities to make greater than one at the window surface. This mechanism has been shown to exist at the cylindrical windows described in reference (1).

- b. The existence of X-rays or other radiation at the window which will liberate electrons from the surface.

When the magnetic fields are used as described it is not hard to explain the restoring force.

It will be seen that all the four windows tested had a different critical field for the start of multipactor without the use of magnetic fields but had the same critical field when magnetic fields were used. This presumably indicates differences in the restoring force for each window without magnetic fields. It cannot be explained by differences in the secondary emission characteristics since the use of the magnetic fields gives identical results for all the windows. Since the windows were all tested at about the same frequency and with the same geometrical configuration, the differences cannot be explained in terms of electric field inhomogeneity forces. The differences must, therefore, be due to differences in the positive charge or differences in the starting conditions. This needs further investigation. One possible explanation is that the incident electron current arriving at the surface is different in each case. This is quite conceivable because each window was processed separately and we would expect the amount of field emitted electrons from the metal surfaces to be different. Another possible explanation is that the electrical conductivity of the window surfaces was different. This would have an effect on the positive static potential built up because of different charge drainage rates over the surface due to the different conductivities.

Concerning (5)

It is interesting that the power dissipated due to the multipactor discharge rises relatively slowly with increasing electric

field strength above the critical field level ($P_d \propto E^{2.6}$ for TU-4). This is in contrast to the cylindrical windows described in reference (1) in which the total dissipated power will usually vary as about the fifth power of the electric field strength above the critical level. It is also interesting that when strong enough magnetic fields are applied to the disc windows, the power dissipated does vary as the fourth or fifth power of the electric field strength. From this we can deduce that the measured dissipation versus electric field characteristic for the S-band windows under discussion depends very largely on the restoring force F as well as on the secondary emission characteristic of the material, and it may be concluded that in a window of this type in the geometry used, the restoring force due to the presumed positive electrostatic charge is not great enough to maintain the multipactor at the maximum power density that could be obtained with higher restoring forces, such as those provided by the added magnetic field. Several interesting conclusions may be drawn from this. First, if the windows tested are, in fact, truly representative of windows attached to high power microwave tubes, then at power levels of the order of a few megawatts the power loss in the multipactor discharge will be only of the same order of magnitude as the power loss in the dielectric due to normal dielectric losses. This presumably accounts for the fact that such microwave tubes do, in fact, work and failures of windows by non-local overheating are relatively rare, at least when the average power level is low.

Second, if the relationship found between power dissipated and electric field strength applies at higher power levels than we used in our tests, then at transmitted powers of the order of several tens of megawatts, the power loss in the multipactor would be many times greater than dielectric loss and, therefore, the multipactor will, in fact, be the limiting factor in the average power handling capacity of the window.

Third, it is conceivable that a window can run with no multipactor, or perhaps a weak

multipactor, not dissipating much power under normal conditions, and that a sporadic condition may occur suddenly which would provide a larger restoring force F. This might increase the power loss and the severity of the multipactor many times and destroy the window.

4.1.3 Window Coating Methods and Controls (General)

Past successful experience has been with vacuum deposition of titanium metal on the window surface and this will be used first on the waveguide windows to produce a low secondary emitting surface on the window.

Vacuum deposition was originally chosen as the method of application of titanium because of its simplicity, the possibility of close thickness control during deposition, and because it has the least possibility of producing areas of excessive deposition and excessive dielectric losses as compared with a variety of other methods one could think of involving paints or solutions applied by various methods.

If the maximum performance of a window is to be achieved in respect to average power through-put, the dielectric losses of the window must not be increased by any significant amount by the coatings. It has been shown that it is possible to change the secondary emitting characteristics of the window without increasing the dielectric losses in cylindrical windows in resonant cavities at 650 Mc. (1)

Greater tolerance of over-all coating losses is permitted in low average power applications than if the average power level is high. It is quite certain, however, that a concentration of losses which could be produced by bad mixing of a paint or by uneven drying, for example, would tend to cause failure at high average powers.

4.1.3.1 Window Coating Method

The vacuum deposition process consists of evaporating titanium metal in vacuum from a titanium filament which is heated to about 1200°C by current from a low voltage 60 cycle ac transformer. The filament is made of alternate turns

of .010" molybdenum and titanium wire wound on .030" diameter molybdenum wire.

A pure titanium wire could be used as well, since the evaporation is done below the melting point of titanium (1812°C) and the molybdenum core is not essential.

The shape of the filament is a circle or star pattern with a diameter about the same as that of the window, and supported by alumina cylinders in three places.

The quality of the vacuum is not critical and evaporations have been done at 10^{-5} Torr and better. A commercial 18-inch jar evaporator which is equipped with an oil diffusion pump and liquid nitrogen trap is used.

Since the films on the dielectric surfaces are less than 100Å thick, there is no adherence or bonding problem such as would occur in thicker deposited films. Neither the quality of the vacuum nor the substrate temperature, nor the deposition technique is critical.

The steps in the window coating process are:

1. Assemble the filament, measuring probe and window holders on the bell jar plate. Make connections to the filament and to the resistance measuring probe.
2. Close the bell jar and pump down to $<1 \times 10^{-5}$ Torr. This should take about 5 minutes.
3. Supply current to the filament and allow vacuum to recover to 1×10^{-5} while the filament is under 1000°C. This usually takes about 30 seconds.
4. Raise filament temperature gradually (in about one minute or less) until the resistance of the window as measured with a megohmmeter drops to the equivalent of 10^{+7} ohms/square. (See more on coating control, Sec. 4.1.3.3.)
5. Turn off filament, open bell jar, remove window.

4.1.3.2 Meta! Coating Methods

Previous work with cylindrical windows has indicated that coating of metal parts adjacent to the window with titanium is necessary to prevent multipactors which exist between metal surfaces. These generate electrons which may heat the window by direct bombardment, and may start and help to maintain the multipactor at the window. This effect will be geometry dependent, and as mentioned above, it is an important effect in cylindrical resonant cavities. It will be of some interest to determine the role of the metal surfaces in waveguide window structures, since there is evidence that at least ~~some waveguide window electron bombardment effects~~ are strongly dependent upon the geometry of the waveguide structure.

Another reason for coating the metal surfaces with titanium is to prevent contamination of the titanium on the window by metals adjacent to the window that may be sputtered or evaporated onto the window during the exhaust process or during tube operation.

Thin films of copper, for example, are commonly found on window surfaces immediately after exhaust. These can be attributed to the deposition and subsequent reduction of volatile compounds such as the chloride and oxide of copper. These films can be thicker than the penetration depth of secondary electrons and, therefore, in addition to adding to the dielectric losses of the window, they will determine the secondary yield of the surface.

The methods used for coating the copper parts in resonant cavities were plating in a molten salt bath at about 850°C or vacuum deposition on either a hot or cold substrate. All methods were apparently effective in producing a clean titanium surface.

It was found that the temperature of the molten salt plating bath was high enough to cause warpage of copper parts and this method was abandoned for this reason. Vacuum deposition could be done with uniform success on hot substrates (400°C) but the heating and cooling

time made the process expensive. Vacuum deposition on cold copper surfaces was satisfactory, if the thickness was controlled to prevent peeling of excessive layers. This last method seems to be the most suitable for parts of uniform shape on which uniform layers can be deposited.

4.1.3.3 Window Coating Control

It will be recalled that although coatings by using evaporated titanium had been successfully used, and although the process of evaporation is basically very simple, the method of controlling coating thickness developed for cylindrical windows was not applicable for round disc windows because of the lack of contacts for resistance measurement, and therefore some further development work in coating control was needed. The first attempt at a satisfactory control method was outlined in the first Quarterly Progress Report. This method consists of actually measuring the secondary emission coefficient of the window surface during the coating process so that the evaporation could be stopped soon after the secondary emission coefficient had fallen below unity. This method is attractive from many points of view. Accordingly, it was tried in a bell jar set-up.

It would found, however, that it is difficult even to obtain a surface with a secondary emission coefficient greater than unity owing to the presence of carbon films which result from the reduction of hydrocarbons by the bombarding electrons used to measure . The amount of oil vapor present in a bell jar can be reduced by various techniques, but it is apparent that the technique of measuring the secondary characteristics would be extremely sensitive to interfering films. Therefore a new approach was conceived, as described below.

Control of the coating thickness has been achieved in the past by evaporation process. This method has been complicated, partly because of the tendency for very thin coatings to change in resistance with time, even while in vacuum, probably because of gas absorption

and the aggregation process; but mainly because of interfering electron and ion currents.

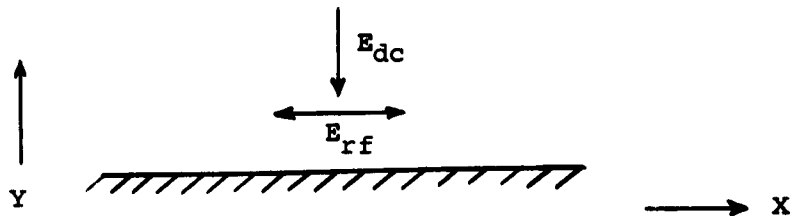
If a resistance of 10^8 ohms/sq. or more is desired, stray currents on the order of 10^{-7} to 10^{-8} amperes have been found to mask the resistance measurements.

A technique has been planned using a metering probe which contains a resistance path of 10^2 squares in parallel between the evaporating filament and the window to be coated. This should reduce the effect of the stray current to an acceptable level. Since this probe will be cleaned after every coating, it was decided to make it of sapphire rod, metallized with moly-manganese. It is hoped that this combination will stand the repeated removal of titanium without damage.

Since it is difficult to design a filament which will produce an exactly uniform and unchanging pattern of deposition, the probe should be placed close in front of the window in order to know accurately what is being deposited on the window. Small variations in thickness of the coating on the window caused by the probe are not expected to be important.

The proposed arrangement is shown in Figure 8.

4.1.4 Mathematical Analysis of Multipactor Motion on a Single Dielectric Surface with No Static Magnetic Field



Let v_0 be the initial velocity of a secondary electron, having components v_{0x} and v_{0y} in the x and y directions.

Let E_{rf} be an alternating electric field parallel to the surface.

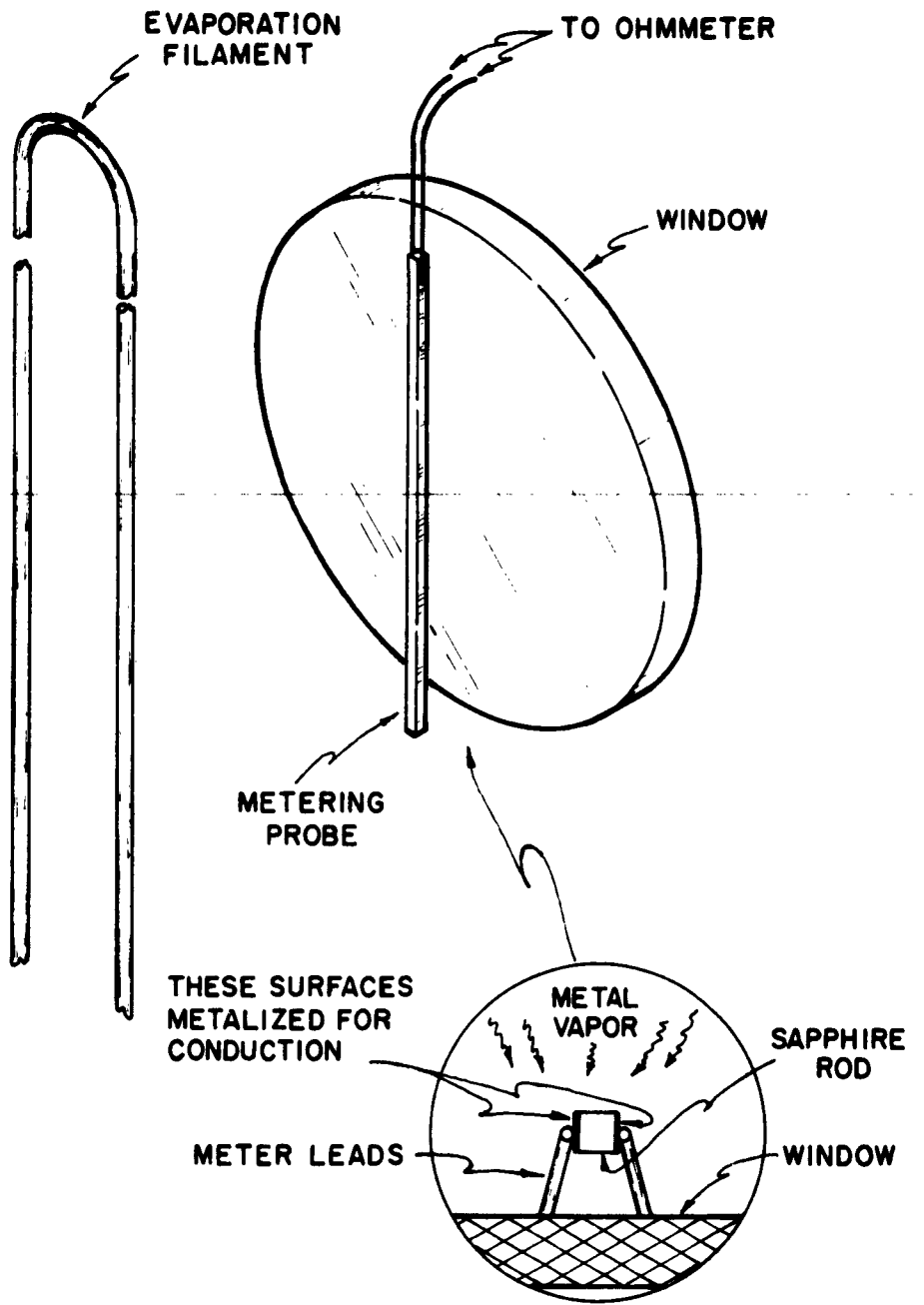


FIG. 8

Let E_{dc} be a static electric field normal to the surface.

The differential equations of motion for an electron will be:

$$\frac{d^2x}{dt^2} = \frac{e}{m} [E_{rf} \sin \omega t] \quad (1)$$

$$\frac{d^2y}{dt^2} = \frac{e}{m} [E_{dc}] \quad (2)$$

where

e is electron charge, m is electron mass, ω is frequency in radians per second.

Also, let

$$\frac{e}{m} \cdot E_{rf} = A,$$

$$\frac{e}{m} \cdot E_{dc} = B.$$

Then, rewriting,

$$\ddot{x} = A \sin \omega t,$$

$$\ddot{y} = B.$$

Also, let t_0 be the time when the electron leaves the surface.

The solutions to these equations are:

$$x = -\frac{A}{\omega^2} [\sin \omega t - \sin \omega t_0] \\ + \frac{A}{\omega} \cos \omega t_0 [\omega t - \omega t_0] + v_{0x} (t - t_0), \\ y = -\frac{B}{2} (t - t_0)^2 + v_{0y} (t - t_0),$$

giving the displacements at time t , and

$$\frac{dx}{dt} = -\frac{A}{\omega} (\cos \omega t - \cos \omega t_0) + v_{0x}$$

$$\frac{dy}{dt} = B(t - t_0) + V_{0y}$$

giving the velocities.

Maximum velocity in the x direction occurs when $\omega t = \pi (2n + 1)$, where n is any integer, and $\cos \omega t_0 = 1$, giving:

$$V_{x \text{ max}} = 2 \frac{e}{m} \frac{E_{rf}}{\omega} + V_{0x}$$

This may be expressed in electron volts V by using the following formula:

$$eV = \frac{1}{2} m v^2$$

In the practical case where the initial velocity of the electron is small compared to its final velocities, the following equation gives a very close approximation to $V_{x \text{ max}}$:

$$V_{x \text{ max}} = 2 \frac{e}{m} \left(\frac{E_{rf}}{\omega} \right)^2 + V_{0x}$$

4.2 CONCLUSIONS

The following conclusions are tentative and need to be supported by further experimental results:

1. Using a normally process alumina or beryllia flat disc window at S-band in a geometrical environment similar to that used on many microwave tubes, a multipactor discharge will tend to occur when the transmitted power is sufficiently high, meaning above about 135 kilowatts peak. This power level should be independent of frequency.
2. The lowest power level at which the multipactor can occur is experimentally found to be very close to that predicted by the theory, which is basically the same theory already developed as a result of work on cylindrical windows. (1)
3. The exact level at which the multipactor will start depends on the individual circumstances including the geometry of the window and its environment prior to testing. For 4 windows tested, the levels were 2.8 MW, 0.1 MW and 0.42 MW.
4. The actual power loss in the multipactor discharge appears to vary as about $E^{2.6}$ where E is the electric field strength, at least up to transmitted power levels of a few megawatts.
5. There may be no difference in the behavior of alumina and beryllia windows regarding critical field strength or dissipation versus field strength characteristics during the multipactor discharge.
6. The multipactor will occur under conditions of high vacuum. The vacuum used in the tests was of the order of 10^{-8} to 10^{-9} Torr.
7. It seems highly probable that a positive electrostatic charge exists at the window surface under typical operating conditions. This charge is the only reason for the existence of the restoring force on electrons required to sustain the multipactor in the absence of a static magnetic

field.

An additional conclusion can be made at this time:

A thin circular disc window of BD 96 beryllia, water-cooled around the periphery, assuming no multipactor, should be capable of transmitting more than 300 KW of average power at 2850 MC without failure due to thermal stress.

4.3 PROGRAM FOR NEXT INTERVAL

4.3.1 Further Testing

We anticipate obtaining a higher pulse klystron generator which will allow the power levels to be raised at least 2 orders of magnitude above those reported herein.

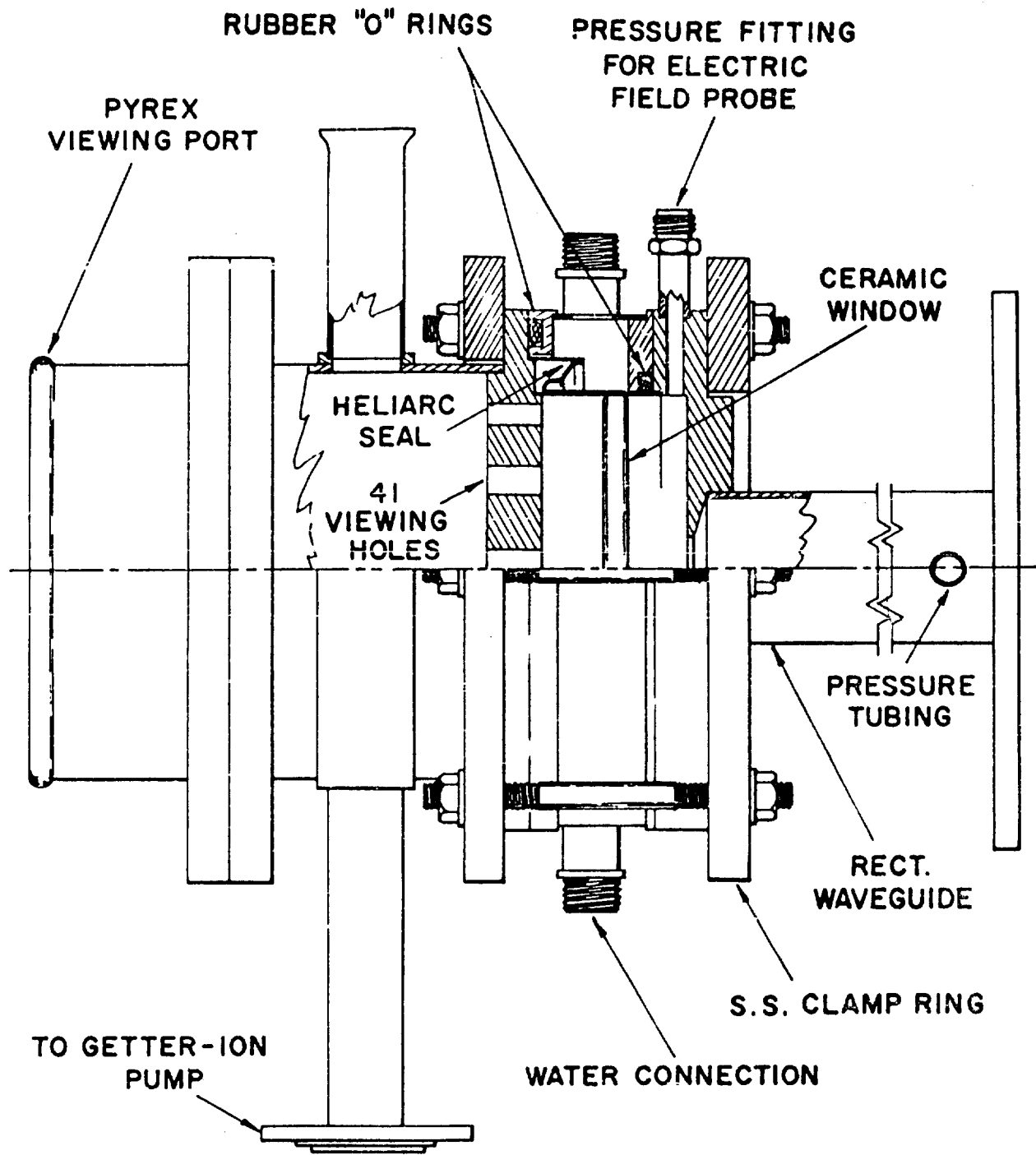
The new window box illustrated in Figure 9 will be used for these tests. This can be pressurized and allows a good view of the vacuum side of the window through the optical window provided. We shall endeavor to observe the glow pattern on the window for several magnetic field configurations, around the critical field level, to give more insight into the exact nature of the electron motions under these conditions.

We shall also coat windows with the evaporated titanium method described herein to see if the multipactor can be suppressed as anticipated. We shall also measure the rf losses introduced by the coating itself, and any other important characteristics.

We shall make measurements on windows prepared by the methods described by Oskar Heil under Task B of this report.

4.3.2 Coating Control

We shall use the thin probes described herein in the existing bell jar for coating control using the resistance measurement method.



"WINDOW BOX" ASSEMBLY - MODEL 2

FIG. 9

If time permits, we shall investigate further the method of control using measurement of the secondary emission coefficient.

5. TASK B

STUDY OF THE INNER-WINDOW SURFACE AND CONFIGURATIONS
AFFECTING POWER HANDLING CAPABILITIES OF HIGH POWER
MICROWAVE TUBES.

Prepared by

Oskar Heil

Oskar Heil

5.1 FACTUAL DATA, PROGRESS TO DATE

During the reporting period, 9 windows were tested. All the work connected with high frequency matching and testing of the windows was done at the facilities of the Stanford Linear Accelerator. Thanks are due to Dr. Lebacqz, J. Jasberg, R. Bierce, D. Soule, and H. Woods for valuable discussions and experimental testing of the windows.

Seven of the windows were alumina (AL300) (Nos. 1-7) and two were silica (Amersil optical grade) Nos. 8 and 9). All these windows had grooved surfaces as described in the previous report with the exception of alumina window No. 7. This window had planar surfaces and dotted coatings of titanium suboxide. Windows No. 1, 2 and 3 (alumina) and No. 9 (silica) had no coatings. All the other windows had the coating only on the crests of the ridges, and flat Window No. 7 had, as mentioned, a network of dots .75 mm apart which covered 20% of the surface area. The results obtained on the 9 windows are shown in Table No. 1.

During testing, the pulse rate is normally 60 per second but is increased up to 240 and 360 pulses per second in order to increase the average power on the window. The highest values obtainable in the Stanford Ring Resonator are approximately 85 MW peak and 15 kW average at 60 pulses, and approximately 40 MW peak and 43 kW average at 360 pulses. In the experiments, it was noticed that windows without multipactor showed no failure with the exception of window No. 5. It was found that this window had bad thermal contact by being loose in the copper waveguide cylinder, which very likely accounts for the failure. All test windows are not metallized, but are shrunk into the copper cylinder where they normally sit tightly in good thermal contact. Window No. 7 showed no multipactor, but had a slight surface damage on each surface. Since the damages were approximately adjacent to one another on the two faces, it was at first believed that a puncture had occurred. The window was removed, photographed, built in again, and run at 85 megawatts for one hour. Leak checking after this treatment showed that it was still vacuum tight. The small surface damage marked by an arrow is shown in Figure 18 in magnifications of 3 and 60 times. With this brief summary of results, a few technical details about manufacturing and coating of windows will be described.

TABLE I

WINDOWS TESTED AT STANFORD
(3 micro-second pulses)

Nr	Material	Surface	Coating	Failure at		Highest Power		Multi-pactor	Remarks
				Peak Ave. MW	Peak Ave. kW	Peak Ave. MW	Peak Ave. kW		
1	AL 300	Grooved	No	34.	6.	34.	6.	Yes	
2	"	"	"	36.	6.5	36.	6.5	"	
3	"	Grooved Sandblasted	"	28.	20.0	78.	14.	"	
4	"	Grooved	Yes	No Failure		85. 40.	15. 43.	No	
5	"	"	"	63.	11.5	63.	11.5	"	Window loose in fitting
6	"	"	Half	No Failure		70.	12.5	"	
7	"	Plain	Dots	No Failure		85. 39.	15. 42.	"	2 Surface Marks
8	Silica	Grooved	Yes	No Failure		87. 39.	15.5 42.	"	
9	"	Grooved	No	No Failure		84. 40.	15. 43.	"	

5.1.1 Grooving of Silica Windows

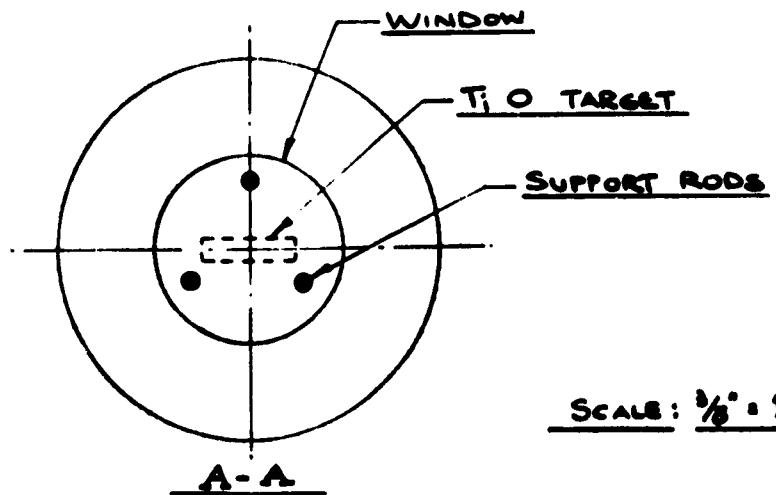
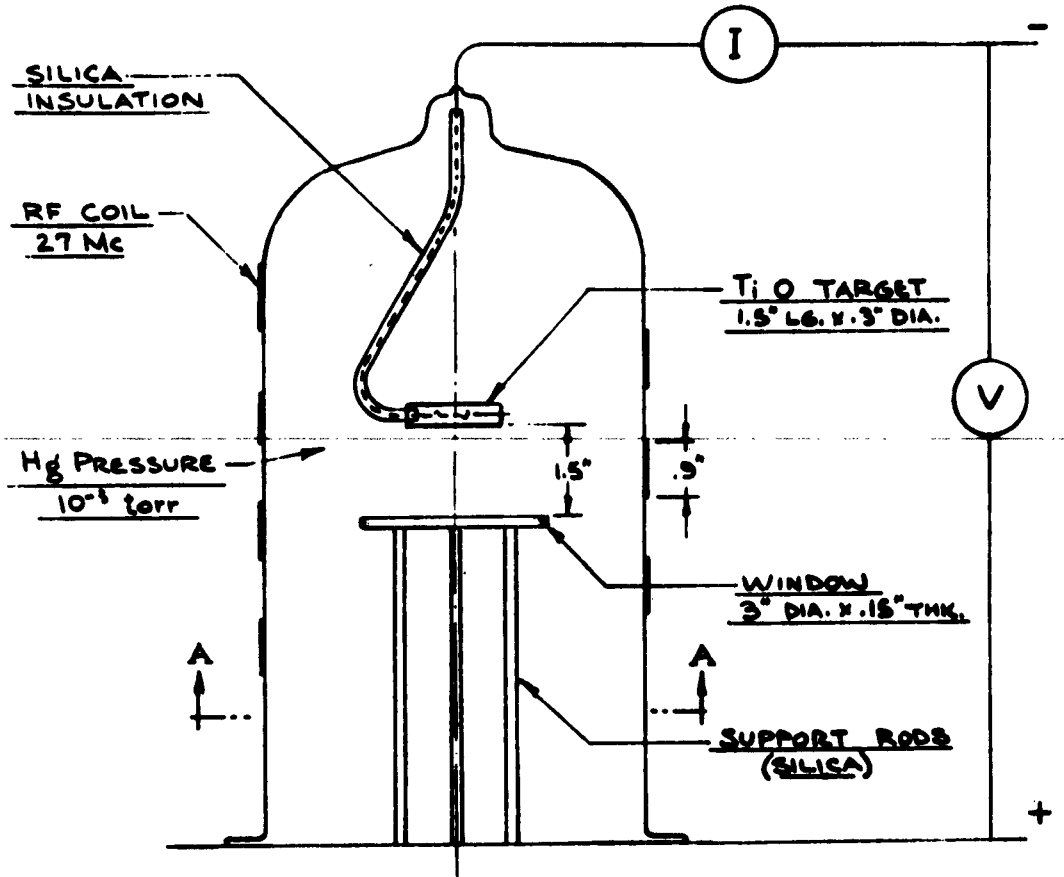
Grooved alumina windows were made by form pressing the powder and sintering the window as described in the previous report. Silica being a much softer material was grooved by grinding both surfaces of a flat 3/16" thick disk of optical grade Amersil. The wear on a V-shaped (90°) 6-inch diameter diamond loaded plastic wheel (Wickman) Type D1 E2 was less than .001" after grinding one side of the window. Before the grooving operation the edge of the window was beveled at 45° to prevent chipping. Figure 17 shows silica window No. 8 on the generator and load side after operating at the highest powers possible and with no visible change on the surface.

5.1.2 Coating by Sputtering

Coatings deposited by sputtering are reproduced much more easily than those by evaporation. The rate of evaporation is temperature-sensitive and can be influenced by surface contamination. The rate of sputtering is temperature-insensitive since the energy of the impinging mercury ions in our case is 1300 eV, which is far above any thermal energy. The sputtered atoms or molecules have energies of several electron volts, also well above thermal energies which leads to firmly bonded coatings without heating the substrate. By keeping the ion voltage constant (1300 volts) and by monitoring current and time in order to obtain the same coulombs, the coatings are reproducible for the same electrode geometry. The geometry used is shown to scale in Figure 10. The rf coil is a copper ribbon wound directly onto the pyrex bell jar. The pressure is kept constant by a cold trap (15°C) between the mercury pump and bell jar. The ion current is held at 4 mA for about 60 minutes. Of course the system shown is only an experimental setup and not the best sputtering arrangement. The sputtering speed can be greatly improved by adding a magnetic field.

The windows were masked during sputtering by laying straight wires in the grooves. Groove width and wire thickness on the alumina windows were 1.3 mm and 0.75 mm, respectively, and 1.5 mm and 0.75 mm

COATING of WINDOW by SPUTTERING



SCALE: $\frac{3}{8}$ " = 1 INCH

FIG. 10
- 40 -

on the silica windows. Silica, however, needs no coating as was shown experimentally.

The masking used for the dotted coating was a nickel wire mesh flattened in a press, which results in a network of dots 0.75 mm apart covering 20% of the area. The amount of TiO sputtered onto the grooved or dotted window was the same in both cases.

5.1.3 Experimental Results with Al 300 Windows

5.1.3.1 Uncoated Windows

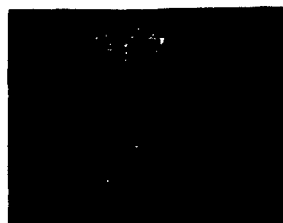
The Stanford Ring Resonator has vacuum on both sides of the window. Lead glass view ports allow visual and photographic observation of the generator and load side of the h.f. window. The surfaces were also viewed through a telescope with a linear magnification of about 7. The temperature of the copper sleeve, holding the window, was also measured. However, this was not a precise calorimetric measurement of the energy dissipated in the window, since the cooling conditions were not controlled. Precise calorimetric measurements are planned in future experiments. The aim of the present experiment was to obtain quick qualitative results as to the existence or nonexistence of the multipactor and to discover more about the nature of the multipactor in regard to window arcing and puncturing. The results with the first three windows were practically identical (see Table 1). There was no multipactor or fluorescence visible near the bottom of the grooves. In the middle of the window the luminosity is symmetrical on both sides of the crests, but in the visible outer parts of the window the slopes show a broader luminosity on the outside than on the inside of the crests.

This indicates that the electrons oscillate parallel to the surface at the center of the window, but at the outside of the window they oscillate at an angle. This field

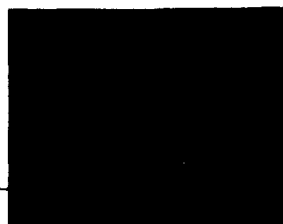
shape is to be expected since the window sits asymmetric in the cylindrical section of the waveguide. It will be shown later (Section 5.1.5) that the sloping incidence of the electrons favors the gliding type of multipactor. Greater luminosity is indeed observed in the outer zones, as shown in Figure 11. This figure contains a series of pictures of window No. 2 taken at intervals during the rise in power. Arc flashes are sometimes observed while raising the power. The camera was therefore left open during this time as shown in the fourth picture of Figure 11. Although the windows were circular, the window views shown are rectangular since the windows are viewed through the neighboring rectangular guides. The little bright spots seems to be loose particles on the surface of the windows. The arcs are arrested by the grooves and do not spread over the surface as already explained in the first quarterly report. It has been found that these light flashes are not connected with any window damage. The multipactor luminosity on the grooved windows is very stable and does not fluctuate. The luminosity distribution over the window surface changes, as the window cavity is tuned, by squeezing the waveguide walls. This is to be expected because of field inhomogeneity pumping due to the variable amount of standing wave energy in the window box.

The first two windows failed at 34 and 36 megawatts because of internal arcing. The failures did not originate at the crests where the multipactor takes place but passed through the bottom of some of the grooves and extended in the direction of the electric field. Such damages are shown in Figures 14 and 18. The damage only seems to be indirectly connected to the multipactor through the temperature rise of the window. It is believed that the puncturing is a run away condition starting at a small overheated spot.

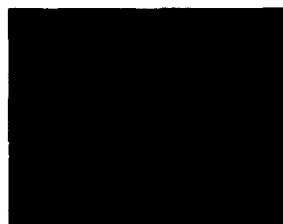
AL 300 GROOVED WINDOW #2, WITHOUT COATING



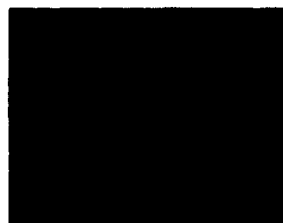
6 MEGAWATTS



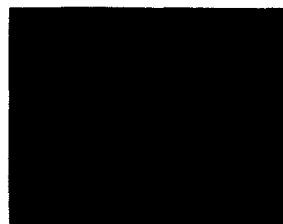
8 MEGAWATTS



10 MEGAWATTS



10-13 MEGAWATTS
(SURFACE ARCING)



35-40 MEGAWATTS



48 MEGAWATTS
(INTERNAL ARCING)



BACKLIGHTED
(WINDOW DAMAGED)

FIG.11

Such a spot might be caused by a localized impurity or by a semi-loose ceramic particle on the surface. A particle which is fully loose will vaporize and disappear without causing damage. Under the microscope semi-loose particles were observed on the bottom of the grooves.

The third window to be tested was first sand-blasted with a fine stream of alumina powder to remove such particles. This window withstood 78 megawatts and failed only after the average power was raised to 20 kilowatts at a pulse power of 28 megawatts (Table 1). The damage is shown in Figure 14.

5.1.3.2 Titanium Suboxide-coated Windows

Window No. 4 was coated by sputtering of TiO₂, only on the crests of the ridges, as described above. The multipactor was dead and the window took all the power of the ring resonator, which was 85 megawatts peak at 15 kilowatts average power and, by increasing the pulse rate, 40 megawatts at 43 kW average power. Window No. 5, which had the identical shape and coating as No. 4, showed no multipactor, but failed by internal arcing at 63 megawatts with 11.5 kW average power. When taking this window out of the ring it was found to be loose in its fitting, as mentioned above, and the failure can be blamed on excess heating of the window. Window Nos. 4 and 5 are shown in Figure 15 after having gone through all the tests. Left is the generator side and right is the load side. The light inclined line on the load side pictures is a small area without coating, which was produced by laying a wire on the window surface, while sputter coating. If the luminosity on the operating window is reduced it can be either due to less electron bombardment or due to reduced capability of the surface to show fluorescence. The shadow area of the line

is too small to influence the multipactor, but it has the original capability to show fluorescence. The damage in window No. 5 is an internal arc in the direction of the electric field. The arc reaches the surface on a few points at the bottom of the grooves. On the generator side the ceramic is chipped. Window No. 6 was grooved, but only coated on half the surface. This coating was the same as on window Nos. 4 and 5. This experiment was done in order to demonstrate visually the killing of the multipactor by the coating. This effect is evident in Figure 12. It is a sequence of luminosity pictures of the window surface while raising the power. The left half is coated, and shows no multipactor. The dark line in the 3 and 5 megawatt picture is the shadow casting of a wire, which held down the mask while sputtering and has nothing to do with the physics of the multipactor. The irregular bright lines which appear in the third and fourth pictures are faults in the photographic material. Ignoring these extraneous factors, we can see how the multipactor killing effect spreads gradually over the whole window surface, ending with a dead window surface. From there on, the window remained dead raising the power up to 70 megawatts or lowering it down to 3 megawatts again. The last picture shows an arcing on the corner of the rectangular waveguide, which illuminated the window with light and some electrons, showing clearly the dividing line between coated and uncoated surface. This arcing happened during the increase of power from 45 to 62 megawatts. The window after being taken out is shown in Figure 16. The load side had the half coating, whereas the generator side was fully coated with exception of the diagonal line as described before. All these windows which were dead in multipactor, showed an X-ray level about two orders of magnitude smaller. When the multipactor was killed, the vacuum in the ring was found to improve by practically a factor ten, to about 3×10^{-6} Torr.

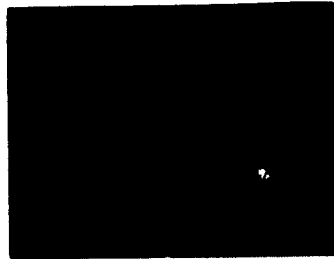
The results of window No. 6, that is the migration of the multipactor quenching effect over the whole surface, suggested the experiment done on window No. 7. The planar, un-grooved surfaces of the Al 300 window were coated only in small dots covering the whole surface, assuming that the multipactor killing effect would spread over the whole area, which it really did. The surface of the window is shown in Figure 17 with the window in the guide after severe testing to 84 megawatts peak at 15 kilowatts average and 39 megawatts peak at 42 kW average. Because of a very small surface damage, which is shown in ~~picture 16 in a magnification of 3 and 60~~ times, the window was put back for more severe treatment. It was then taken out with no further damage and is shown in Figure 16.

5.1.4 EXPERIMENTAL RESULTS WITH SILICA WINDOWS (AMERSIL, OPTICAL GRADE)

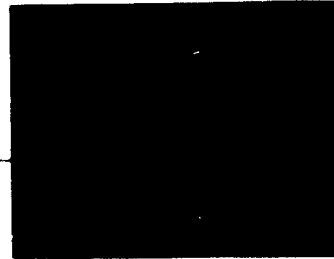
Two grooved silica windows were tested. Window No. 8 had titanium suboxide coating on the crests like the Al 300 windows, and window No. 9 had no coating. Both windows were free of multipactor and withstood the tests to highest peak and average powers as shown in Table 1. Figure 17 shows window No. 8 after testing with no visible change. The chipping, noticeable on the window edge, happened in the grinding operation. Figure 13 shows window No. 9, that is, the uncoated window, in operation. With very long exposures (40 sec f 32 ASA 3000) a faint luminosity at the lower power levels can be observed, which disappears completely at higher energy levels. The fourth picture shows the reflection of a waveguide arc in the granular structure caused by the grinding of the grooves. The last picture had an exposure time of 3 minutes at f 8 with a film sensitivity of ASA 3000.

It is surprising that silica can take the high average power of 43 kilowatts with vacuum on both sides in spite of its relatively small heat conductivity. Mention should be made here about the dielectric loss

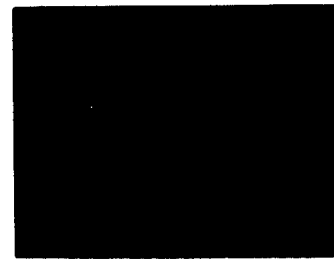
AL 300 GROOVED WINDOW #6 HALF COATED WITH TiO₂



3 MEGAWATTS



5 MEGAWATTS



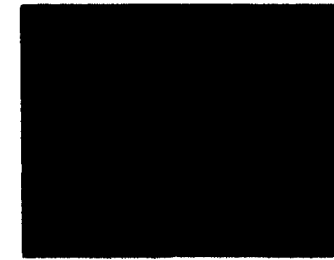
6-9 MEGAWATTS



11-18 MEGAWATTS



15 MEGAWATTS



45-52 MEGAWATTS

FIG.12

values obtained by Westphal on Amersil optical grade silica, which show a drop in $\tan \delta$ from the room temperature value (1.5×10^{-4}) to less than half (0.6×10^{-4}) at 600°C , the room temperature value being reached again only at about 820°C .

Lower secondary emission in silica makes it possible to have no multipactor on grooved windows without coatings. An explanation might be the fact that silica shows a strong electron bombardment induced conductivity⁽²⁾. This conductivity reduces the micro-field within the insulator and with it the amount of secondaries emitted. Fast electrons penetrating an insulator yield a net negative charge at the end of their range. Slow electrons hitting the surface causing secondary emission create a positively charged surface. The field between these two charged layers tends to accelerate electrons towards the surface where they can be emitted as secondaries. This happens only if the induced conductivity is not too great, because too many electrons will discharge this field and there will be no enhancement of secondary emission.

(2) L. Pensak, Phys, Rev. V. 75, p. 472, Conductivity Induced by Electron Bombardment in Thin Insulating Films.

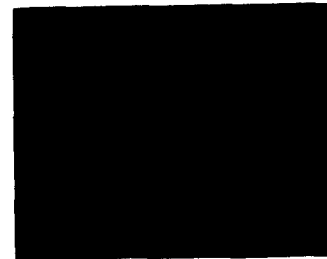
SILICA WINDOW #9 WITHOUT COATING



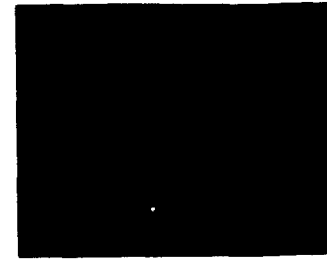
3-5 MEGAWATTS



9-14 MEGAWATTS



18-24 MEGAWATTS



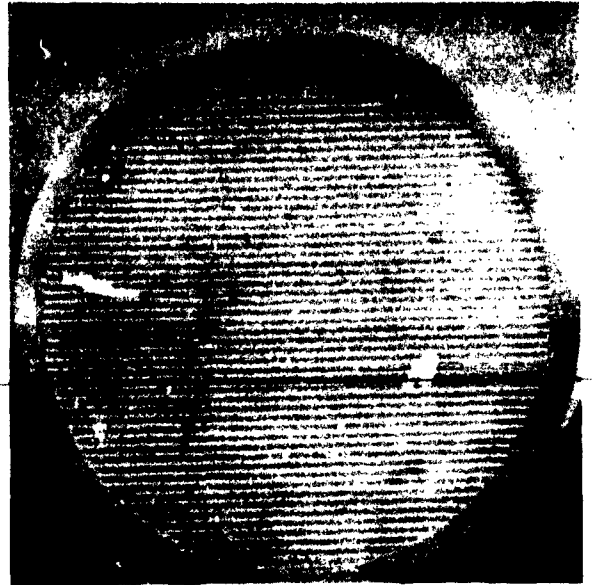
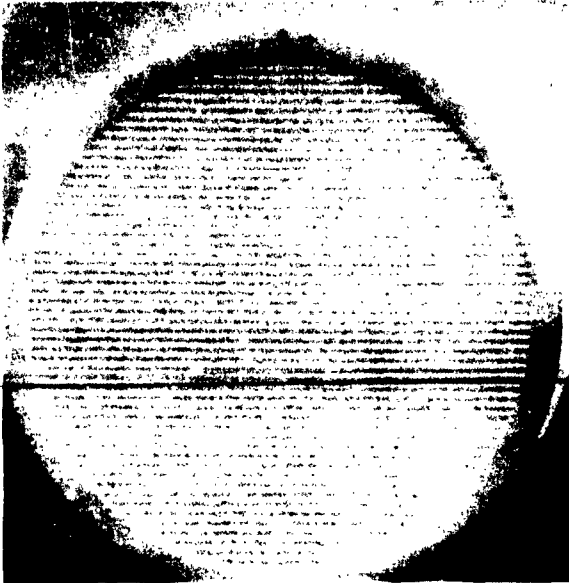
30-43 MEGAWATTS
(WINDOW ILLUMINATED
BY ARC IN WAVEGUIDE)



84 MEGAWATTS

FIG.13

WINDOW NO. 1 (AL 300)



WINDOW NO. 3 (AL 300)

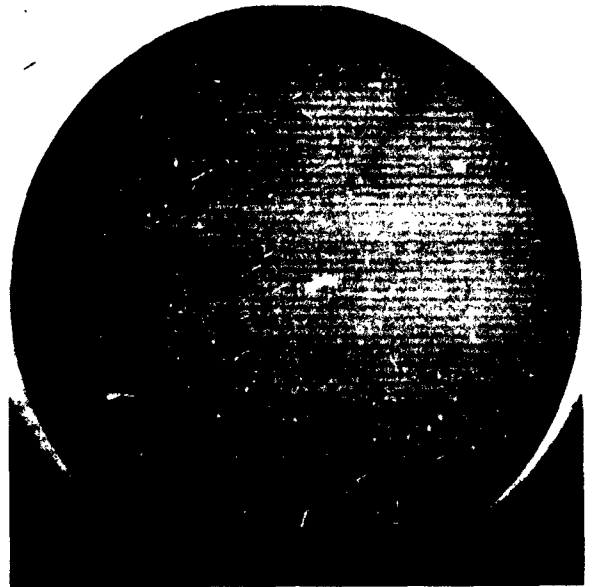
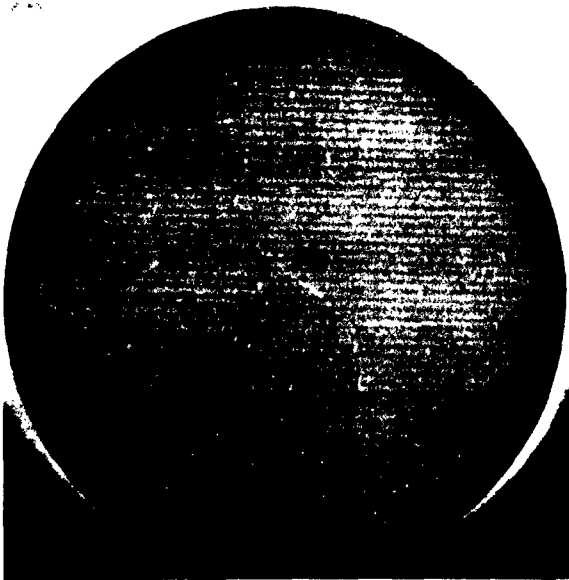
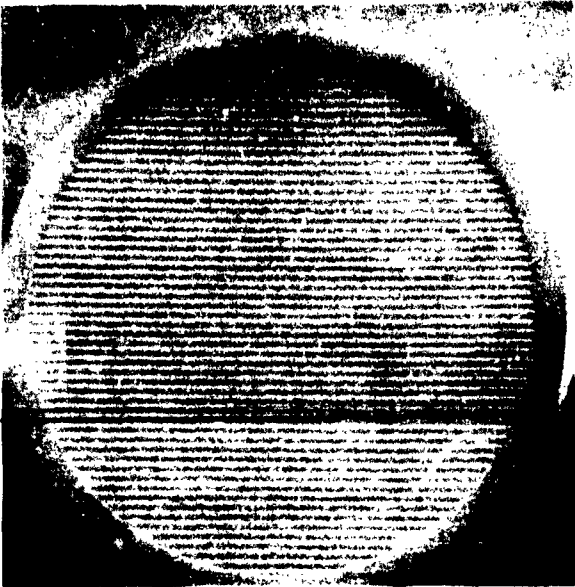


FIG. 14

WINDOW NO. 1 (AL 300)



WINDOW NO. 3 (AL 300)

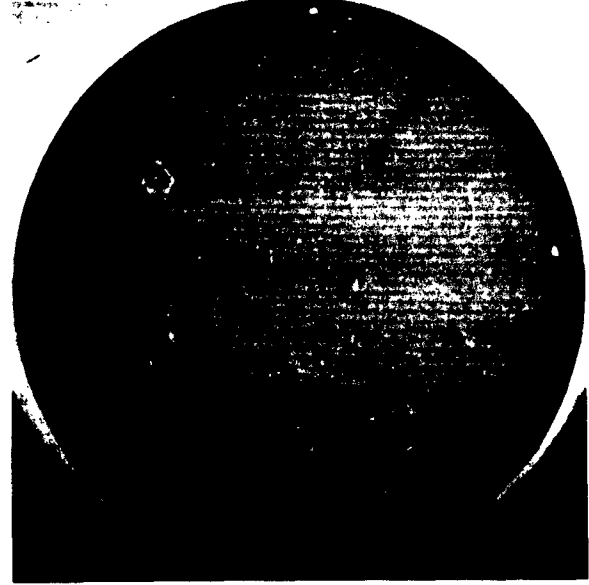
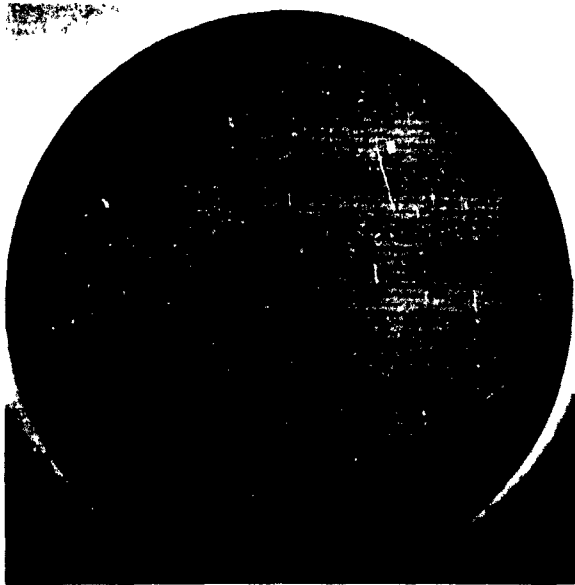
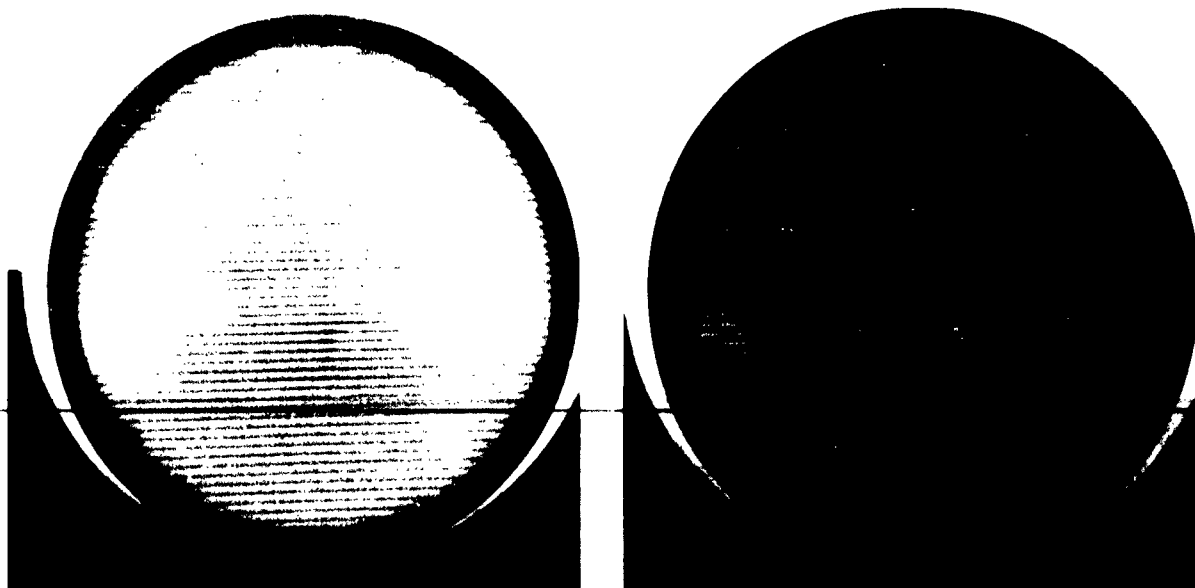


FIG. 14

WINDOW NO. 4 (AL 300)



WINDOW NO. 5 (AL 300)

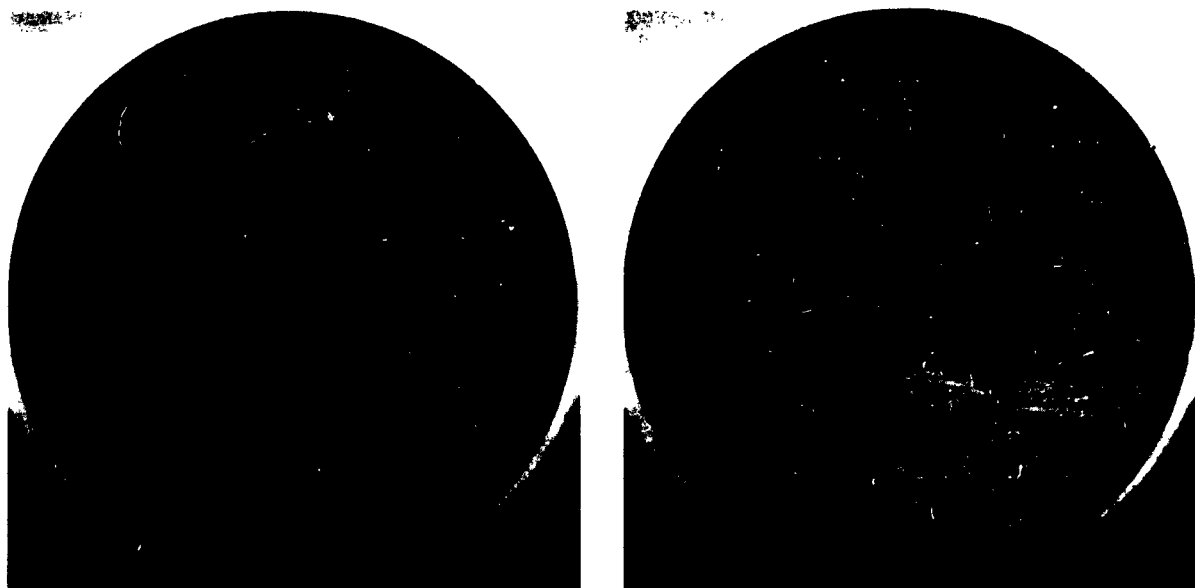
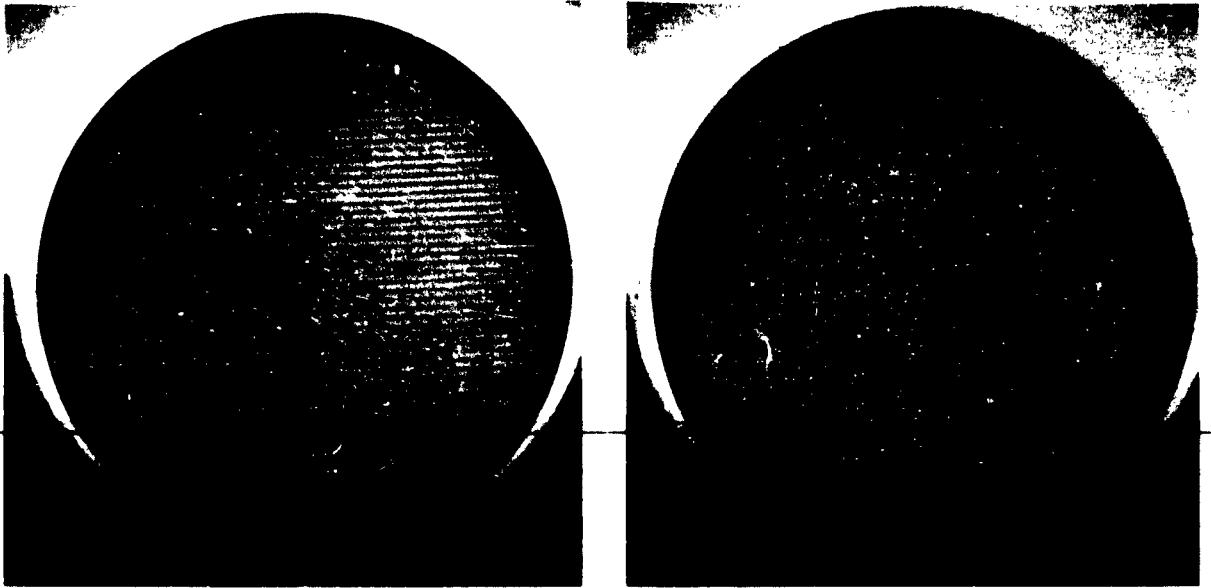


FIG.15

WINDOW NO. 6 (AL 300)



WINDOW NO. 7 (AL 300)

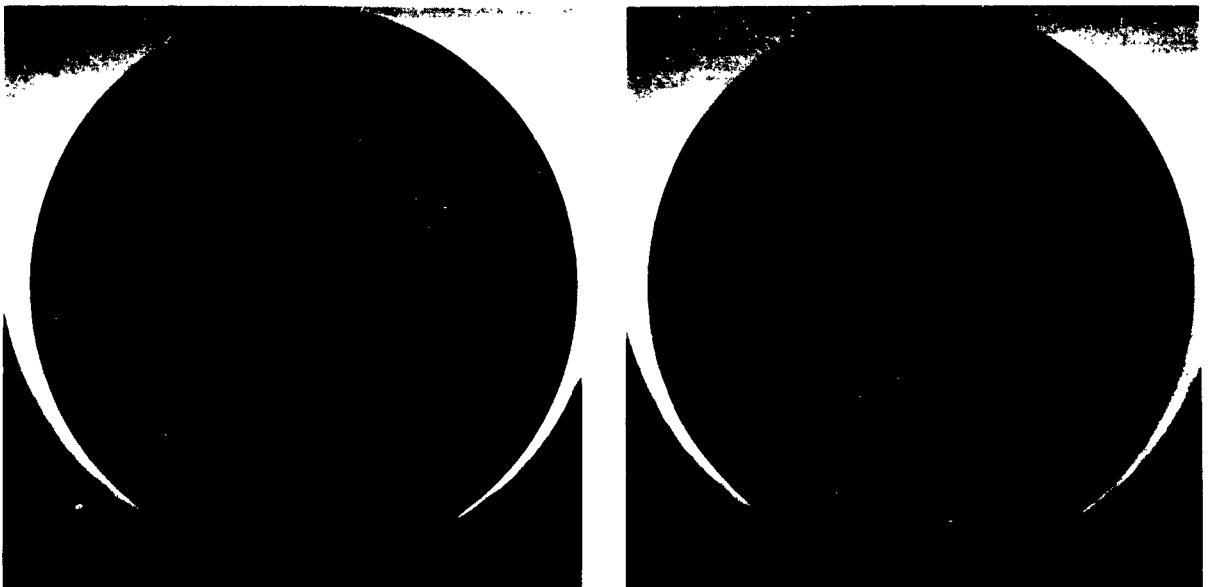
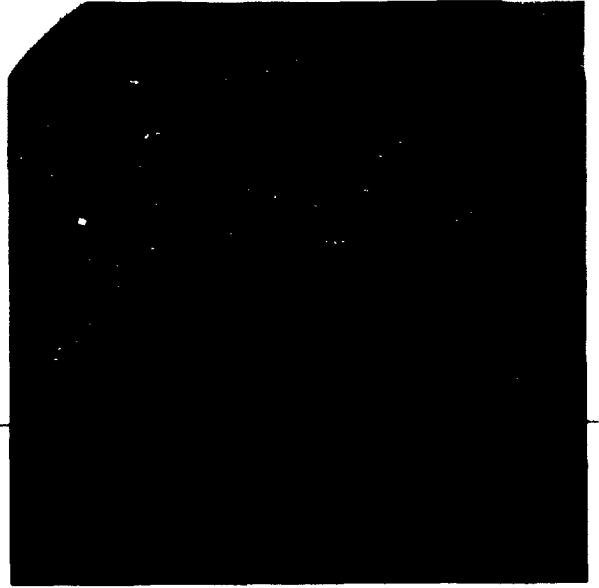


FIG.16

WINDOW NO. 7 (AL 300)

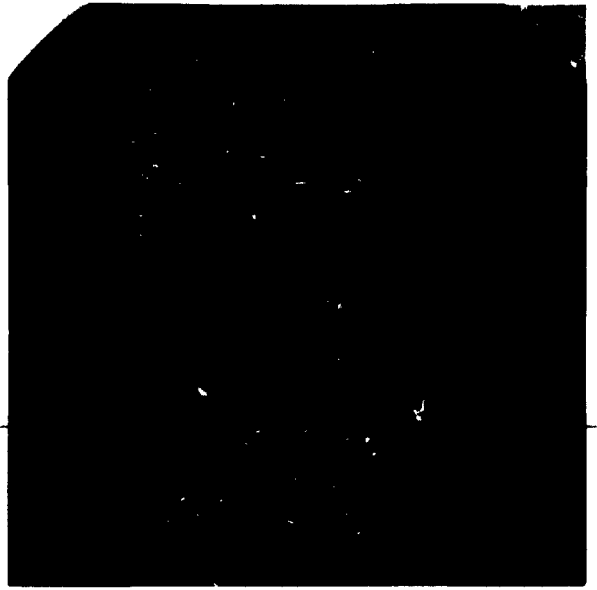
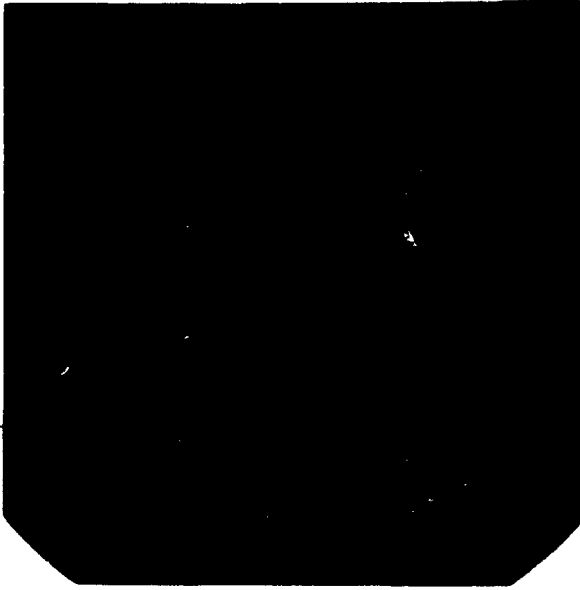


WINDOW NO. 8 (AMERSIL, OPTICAL GRADE)



FIG.17

WINDOW NO. 7 (AL 300)



WINDOW NO. 8 (AMERSIL, OPTICAL GRADE)

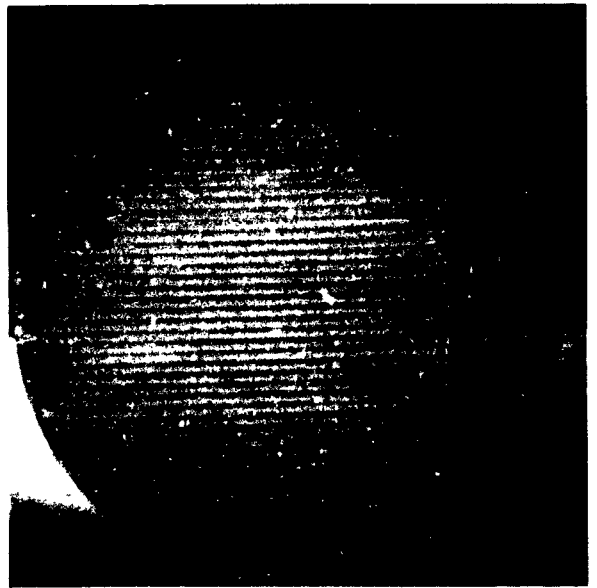
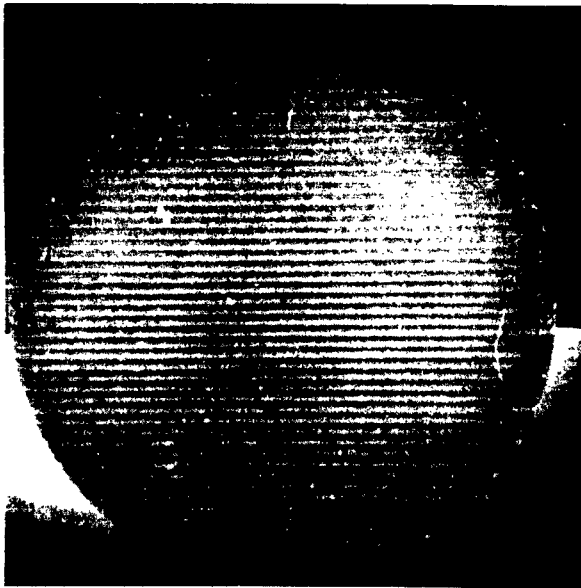
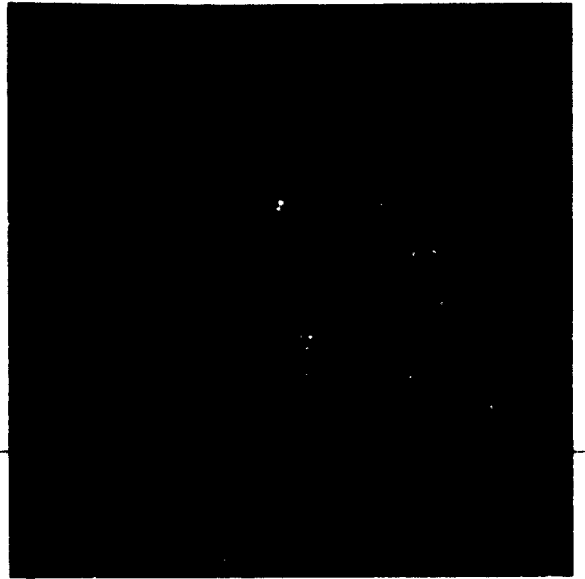


FIG.17

WINDOW NO. 7 (AL 300)

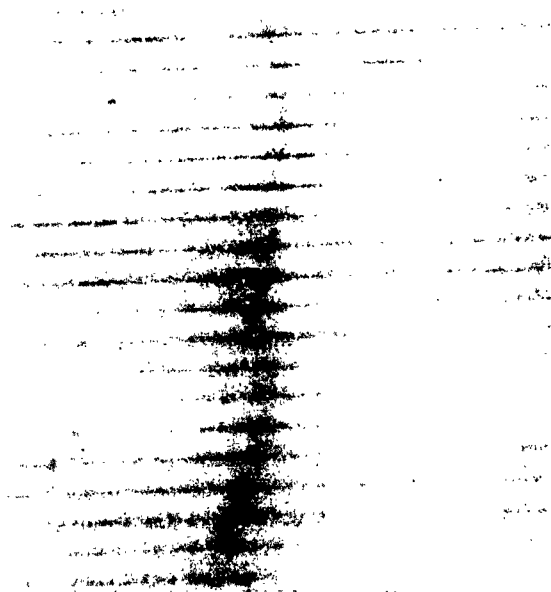


3 X

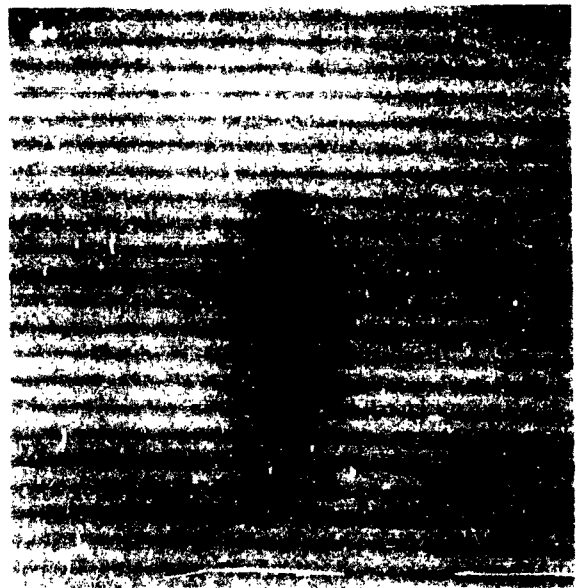


60 X

WINDOW NO. 1 AND 2



3.5 X



3.5 X

FIG.18

5.1.5 PHASE-SELECTED SECONDARY EMISSION BY OBLIQUE ELECTRON OSCILLATIONS

If electrons oscillate in a slightly oblique angle to a surface and slowly approach this surface, they will always hit this surface at about the same phase, namely at one peak of their amplitude. In all the other parts of their cycle they have a greater distance from the plane. Secondary electrons will be released at that moment. The moment of peak amplitude is also the moment of peak electric field for a free electron oscillating in an alternating field. We have shown in the last quarterly report (see Figure 12) that an electron released at the peak of the field will oscillate stationary, i.e., with no net d-c velocity, released at zero field will move with a d-c velocity equal to its peak a-c velocity. Electrons with d-c velocities move out of the multipactor region and tend to quench the multipactor. Since these "quenching" electrons in the above geometry represent only a small percentage of the total electrons present, the resulting multipactor becomes more intense. Oblique incidence and greater intensity were observed in combination as described earlier.

5.1.6 EFFECTS ON ELECTRONS IN DIRECTION OF POWER FLOW
(RADIATION PRESSURE)

Let v be the instantaneous velocity in the direction perpendicular to the propagation of an electromagnetic wave obtained by an electron from the field. Since the corresponding kinetic energy is supplied by the propagating wave, this amount of electromagnetic energy is missing from the wave. Expressed in terms of the electron mass m , the equivalent mass of the missing energy is $mv^2/2c^2$ (for non-realistic electron velocities). But in this exchange process not only the energy is conserved but also the momentum attached to this energy. The electromagnetic energy absorbed by the electron has the above-mentioned mass

$$\frac{m}{2} \frac{v^2}{c^2}$$

and the velocity of the energy propagation of the wave, which is c for a planar wave and the group velocity c .

$$\frac{\lambda}{\lambda_g}$$

in a waveguide wave (λ is the free wave length and λ_g the guide wave length). The momentum of the wave, mass x velocity, must equal the forward momentum of the electron:

$$\frac{m v^2}{2 c^2} \cdot c \frac{\lambda}{\lambda_g} = m v_f$$

where v_f is the forward component of the electron velocity. We obtain for the forward velocity of the electron

$$v_f = \frac{v^2}{2c} \cdot \frac{\lambda}{\lambda_g} \text{ or } v_f = v \frac{\beta}{2} \cdot \frac{\lambda}{\lambda_g} \text{ with } \beta = \frac{v}{c}$$

For the free wave $\frac{\lambda}{\lambda_g}$ becomes one and disappears out of the equations.

If we express the kinetic energy of the electron in direction of the field in electron volts as Ue , and the kinetic energy in the forward direction as $U_f e$ we obtain the following:

$$\frac{m v_f^2}{2} = U_f e = \frac{m v^2}{2} \cdot \left(\frac{v \lambda}{2c \lambda_g} \right)^2 = U e \cdot \left(\frac{v \lambda}{2c \lambda_g} \right)^2$$

$$\text{or } U_f = U \left(\frac{v \lambda}{2c \lambda_g} \right)^2 = U \left(\frac{\beta \lambda}{2 \lambda_g} \right)^2$$

$$\text{since } U = \frac{m v^2}{2 e} ; v^2 = U \frac{2 e}{m}$$

$$U_f = U^2 \frac{e}{2 m c^2} \left(\frac{\lambda}{\lambda_g} \right)^2$$

$$\text{for } e = 1.602 \times 10^{-12} \text{ erg. } v^{-1}$$

$$m = 9.107 \times 10^{-28} \text{ g}$$

$$c = 2.998 \times 10^{10} \text{ cm sec}^{-1}$$

$$U_f = 9.7795 \times 10^{-7} U^2 \left(\frac{\lambda}{\lambda_g} \right)^2$$

It can be seen that the forward energy of the electron in electron volts is proportional to the square of the electron energy in the direction of the E field. This relation is of course valid for any moment during the oscillating cycle, because the law of conservation of energy and momentum is valid at any moment. Figure 19 shows, in the bottom row, electron velocities in the E field direction for electrons released at different phase angles and therefore having different mean d-c velocities added to the a-c velocity. The phase angles at the time of release of the electrons are given. These were chosen to yield d-c velocity rises in five equal steps from picture to picture. The resulting forward velocities are shown in the top row.

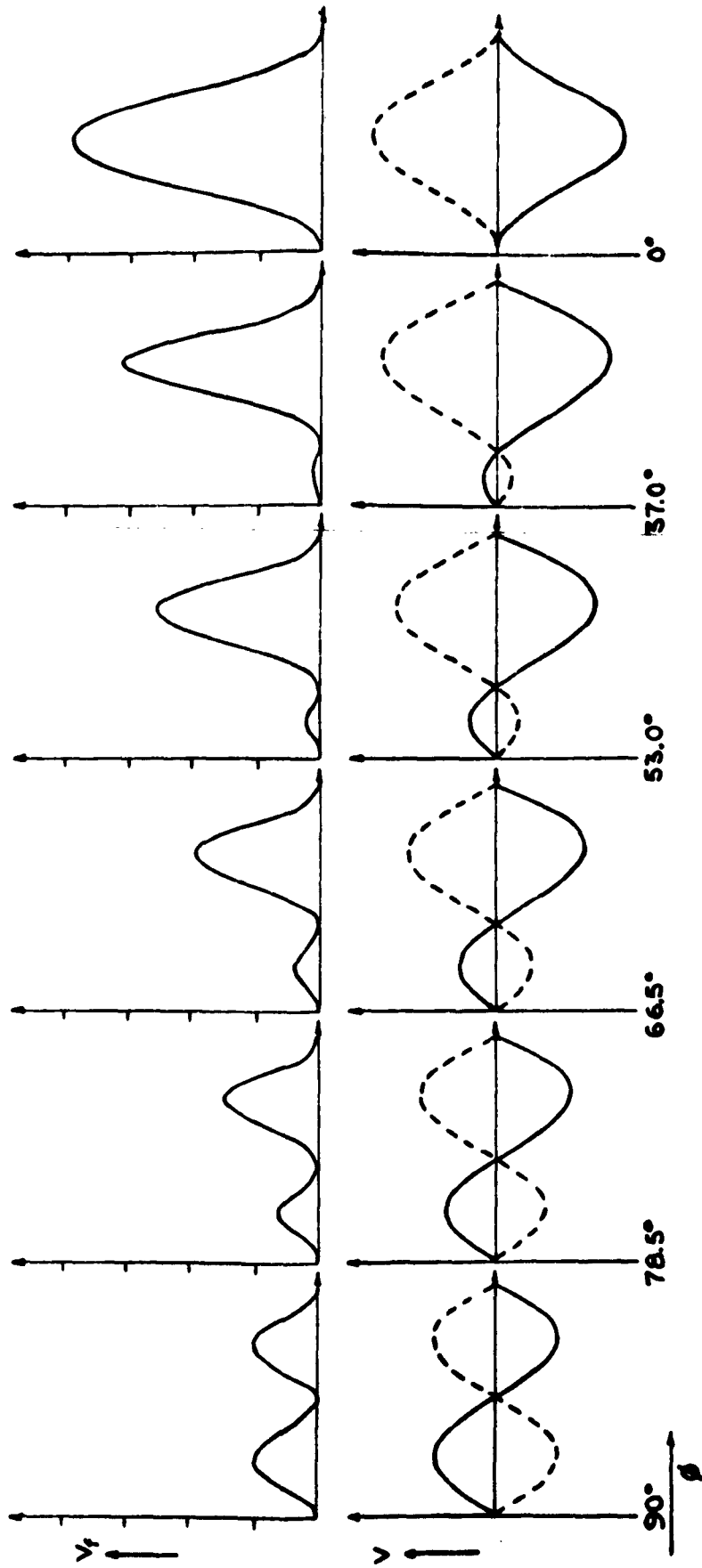


FIG. 19

We recognize the frequency doubling effect in v_f due to the square relationship in the first case and we see that more of the fundamental frequency gets mixed in, as the d-c velocity in the bottom row grows, until finally the mixed-in fundamental has reached twice the amplitude of the second harmonic, which remains constant in amplitude through all the pictures. The peak forward velocity at 0° phase angle is four times that for 90° , with all intermediate values possible, which means energy-wise a factor of sixteen. Similar electron motions have been computed by D. Churchill using an analogue computer⁽³⁾.

The energy U of the oscillating electron is proportional to the square of the electric field and for that reason U_f , the forward energy, goes up with the fourth power of the electric field. The peak energy U of an electron oscillating without d-c velocity in a high frequency field with a peak value of E_p is:

$$U = \frac{e}{2m} \left(\frac{E_p}{\omega} \right)^2$$

This formula is obtained by looking at the momentum $m v$ given to the electron during a quarter of a cycle which equals the average force acting on the electron $(e E_p) \cdot \left(\frac{2}{\pi} \right)$ multiplied with the time $\frac{1}{4v}$:

$$eE_p \cdot \frac{2}{\pi} = \frac{1}{4v} = \frac{eE_p}{\omega} = m v$$

The energy of the electron is:

$$\frac{\text{Momentum}^2}{2 m} = U e = \left(\frac{eE_p}{\omega} \right)^2 \frac{1}{2 m}$$

(3) Sperry Gyroscope Co., Electron Tube Divn., Great Neck, N.Y.
 "Investigation of Microwave Window Failure Mechanisms and Their Elimination", Second Quarterly Progress Report, U. S. Army Signal Research and Development Lab, Fort Monmouth. Contract No. DA-36-039 SC-78314, covering period 1 September 1959 - 1 December 1959, prepared by D. Churchill.

giving⁽⁴⁾:

$$U = \frac{e}{2m} \left(\frac{E_p}{\omega} \right)^2$$

In units: Volt, cm, sec this becomes numerically:

$$U = 8.790 \times 10^{14} \left(\frac{E_p}{\omega} \right)^2$$

$$U = 2.2265 \times 10^{13} \left(\frac{E_p}{v} \right)^2$$

For the peak forward equivalent volts of the electron we obtain:

$$U_f = \left(\frac{e}{2m} \right)^3 \frac{1}{c^2} \left(\frac{E_p}{\omega} \right)^4 \left(\frac{\lambda}{\lambda_g} \right)^2$$

and numerically:

$$U_f = 7.570 \times 10^{23} \left(\frac{E_p}{\omega} \right)^4 \left(\frac{\lambda}{\lambda_g} \right)^2$$

or

$$U_f = 4.857 \times 10^{20} \left(\frac{E_p}{v} \right)^4 \left(\frac{\lambda}{\lambda_g} \right)^2$$

In order to give an idea of the magnitude of this effect, some numerical values, closely related to our experimental conditions, are given in Table II.

(4) These results differ from those presented on page 31 of this report as the results shown here are for electrons with no d-c velocity whereas those on page 31 are for electrons with maximum forward d-c velocity, giving the factor of 4 between the two equations.

TABLE II

85 M-watt Through a Window Area of 45.6 cm²
(3" diameter round window)

	<u>Free Planar Wave</u>	<u>Round Waveguide (TE₁₁)</u>
Wavelength	λ 10.5 cm	λ_g 17.78 cm
Peak-E-Field on Axis	26700. Volt/cm	70600. Volt/cm
Peak-H-Field on Axis	89. Gauss	172.3 Gauss
<u>For an Electron Liberated at Peak of E-Field:</u>		
Max e.V in direction of E	1946. eV	13606. eV
Max e.V perpendicular to E (Radiation Pressure)	3.62 eV	63.25 eV
Amplitude (peak-to-peak)	0.292 cm	0.773 cm
Peak β of electron	8.72%	23.06%
<u>For an Electron Liberated at Zero E-Field:</u>		
Max e.V in direction of E	7796. eV	54600. eV
Max e.V perpendicular to E	58.2 eV	1012. eV
Distance Traveled per half cycle	0.325 cm	0.861 cm
Peak β of Electron	17.45%	46.7%

The first column shows a planar wave carrying an energy of 85 megawatts per 45.6 cm^2 which is the area of a 3-inch window. The second column represents the values in a round 3-inch waveguide TE_{11} mode. The window is assumed to be thin having no standing wave energy surrounding it. For a resonant window having a Q of about three and sitting in the middle of the window box, the forward energies have to be multiplied by Q to give the real values. To understand this we have to look at the peak E-field, which is greater by the factor Q, whereas the peak H-field retains its old value, because the standing wave has no magnetic field in the middle of the cavity. ~~The oscillating energy of the electron is greater by the factor three.~~ However, since the magnetic deflection of the electron into the forward direction results from an H-field, which is not increased, the forward energy increases in this case only proportional to the oscillating energy, that is, by the factor three. We have up to this case, always intentionally ignored the magnetic field deflection which is, of course, responsible for all forward motions and we have used the simpler law of conservation of momentum. But we can also look in the last case only at the momentum transfer and get the right answer. The presence of the standing wave energy in the window box reduces locally the group velocity of the propagating wave. The energy transport velocity is smaller. For the same power flux this means an increased momentum of the electro-magnetic wave. The standing wave energy in the window box is longitudinal. But going from the planar wave to the waveguide wave we also add some standing wave energy in the transverse direction, which is responsible for the reduced group velocity in the waveguide. It is known that the waveguide wave can be understood as two planar waves cutting the guid axis in the angle α where $\cos \alpha = \frac{\lambda}{\lambda_g}$. The electric fields of the two waves add directly to the axis, whereas the magnetic fields combine vectorially to a field value reduced by the factor $\cos \alpha$ or $\frac{\lambda}{\lambda_g}$. The overbalance of the electric field over the magnetic field stems from the standing wave energy, which in this case is transverse to the waveguide, but has

the same effect as the longitudinal standing wave in the window box. We obtain the same forward effect on the electrons either looking at the momentum connected with the group velocity or at the unbalance of electric and magnetic field. The factor in both cases is $\frac{\lambda g}{\lambda}$. The values

in Table II are non relativistic. Only for the rather energetic electrons in the waveguide released at zero E-field does the relativistic effect make a small difference. All the electron energies given for the waveguide case are by a factor Q bigger in the window box. Q is about 3 for the alumina windows and considerably less for silica windows. The forward effects on electrons grow very rapidly with energy and relativistic treatment becomes necessary. Very roughly we can say, an electron which would receive 511 kV energy, that is the relativistic energy-equivalent of the electronic mass, would have forward energies comparable to transverse energies, because the momentum of the radiation absorbed by the electron and the momentum of the electron become the same.

The conclusion can be drawn that the radiation pressure effects on electrons can be neglected at low powers, but become at higher power levels of such magnitude that the electron energies exceed the average velocities of secondary electrons, which greatly affects the nature and magnitude of the multipactor discharge. On output windows, it tends to suppress and on input windows it tends to favor multipactor. Electrons get lifted off the window surface by this effect on the input window and carried back by the d-c charge field of the surface, which is always stronger than the radiation effect. Electrons have, during that time a chance to pick up oscillating energy from the field to effectively knock out new secondaries. On the output window the radiation pressure plus the d-c field tend to bring electrons back rather quickly.

5.2 CONCLUSIONS

5.2.1 Multipactor on windows has been eliminated in three different ways:

- (a) By grooving the surface of silica windows.
- (b) By grooving the surface of alumina windows and coating the ridges of the grooved windows with titanium suboxide.
- (c) By the use of planar windows and coating the surfaces with a discontinuous dotted coating of titanium suboxide.

5.2.2 With the multipactor eliminated by any of the three methods, windows are not destroyed or punctured by the maximum powers of the Stanford Ring Resonator that is, 85 megawatts peak power at 15 kilowatts average, and 40 megawatts peak power at 43 kilowatts average.

5.2.3 It is shown how electron oscillations oblique to the window surface favor multipactoring.

5.2.4 Radiation pressure effects on electrons grow with the fourth power of the propagating wave field strength. It acts in the direction of the power flow and becomes at the consider power levels big enough to have distinct effects on multipactoring. It disfavors multipactor on the generator side of the window and favors multipactor on the load side of the window. However, the effect of inhomogeneity pumping of electrons can over-shadow this effect and reverse its direction. Results obtained by Churchill are of this kind.

5.3 PROGRAM FOR NEXT INTERVAL

Tests are planned on planar silica windows with dotted titanium-suboxide coating, on sand-blasted planar silica, and on grooved beryllia windows. Since grooved silica needs no coating, besides further confirming experiments of the same kind, it is planned to coat grooved alumina and perhaps grooved beryllia windows with silica or silicon-monoxide which is converted into silica on the surface by heating in air.

IDENTIFICATION OF KEY TECHNICAL PERSONNEL

The hours worked by all those participating in the program are:

<u>TASK A</u>	<u>MAN HOURS</u>
D. Preist	253.0
R. Talcott	63.5
J. Zegers	344.0
B. Hill	82.0
K. Scholz	128.0
J. Leidigh	56.0
I. Coutts	103.5
A. McConn	20.0
 <u>TASK B</u>	
O. Heil	120.0
B. Morozovsky	79.5
S. Zott	40.0

IDENTIFICATION OF KEY TECHNICAL PERSONNEL

The hours worked by all those participating in the program are:

<u>TASK A</u>	<u>MAN HOURS</u>
D. Preist	253.0
R. Talcott	63.5
J. Zegers	344.0
B. Hill	82.0
K. Scholz	128.0
J. Leidigh	56.0
I. Coutts	103.5
A. McConn	20.0
<u>TASK B</u>	
O. Heil	120.0
B. Morozovsky	79.5
S. Zott	40.0

REVISED DISTRIBUTION LIST

<u>Contract DA 36-039 SC-90818</u>	<u>No. of Copies</u>
OASD (R&E) Attn: Technical Library Room 3E1065, The Pentagon Washington 25, D.C.	1
Commander Armed Services Technical Information Agency Attn: TISIA Arlington Hall Station Arlington 12, Virginia	20
Advisory Group on Electron Devices 346 Broadway New York 13, New York	2
Director U. S. Naval Research Laboratory Attn: Code 2027 Washington 25, D. C.	1
Commanding Officer & Director U. S. Navy Electronics Laboratory San Diego 52, California	1
Chief, Bureau of Ships Department of the Navy Attn: 681A-1 Washington 25, D. C.	1
Commander Aeronautical Systems Division Attn: ASAPRL Wright-Patterson AFB, Ohio	1
Commander, AF Cambridge Research Laboratories Attn: CRZC (1 cy) L. G. Hanscom Field Bedford, Massachusetts	1

Page 2

No. of Copies

Commander Air Force Cambridge Research Laboratory Attn: CRXL-R, Research Library L. G. Hanscom Field Bedford, Massachusetts	1
Commander Rome Air Development Center Attn: RAALD Griffiss Air Force Base, New York	1
AFSC Scientific/Technical Liaison Office U. S. Naval Air Development Center Johnsville, Pennsylvania	1
Chief of Research and Development Department of the Army Washington 25, D. C.	1
Chief, U. S. Army Security Agency Arlington Hall Station Arlington 12, Virginia	2
Deputy President U. S. Army Security Agency Board Arlington Hall Station Arlington 12, Virginia	1
Commanding Officer U. S. Army Electronics Research Unit P. O. Box 205 Mountain View, California	1
Commanding Officer Harry Diamond Laboratories Connecticut Ave. & Van Ness St., N.W. Attn: Library, Rm. 211, Bldg. 92 Washington 25, D. C.	1
Commander U. S. Army Missile Command Attn: Technical Library Redstone Arsenal, Alabama	1

Page 2

No. of Copies

Commander Air Force Cambridge Research Laboratory Attn: CRXL-R, Research Library L. G. Hanscom Field Bedford, Massachusetts	1
Commander Rome Air Development Center Attn: RAALD Griffiss Air Force Base, New York	1
AFSC Scientific/Technical Liaison Office U. S. Naval Air Development Center Johnsville, Pennsylvania	1
Chief of Research and Development Department of the Army Washington 25, D. C.	1
Chief, U. S. Army Security Agency Arlington Hall Station Arlington 12, Virginia	2
Deputy President U. S. Army Security Agency Board Arlington Hall Station Arlington 12, Virginia	1
Commanding Officer U. S. Army Electronics Research Unit P. O. Box 205 Mountain View, California	1
Commanding Officer Harry Diamond Laboratories Connecticut Ave. & Van Ness St., N.W. Attn: Library, Rm. 211, Bldg. 92 Washington 25, D. C.	1
Commander U. S. Army Missile Command Attn: Technical Library Redstone Arsenal, Alabama	1

Commanding Officer
U. S. Army Electronics Command
Attn: AMSEL-AD
Fort Monmouth, New Jersey 3

Commanding Officer
U. S. Army Electronics Materiel Support Agency
Attn: SELMS-ADJ
Fort Monmouth, New Jersey 1

Corps of Engineers Liaison Office
U. S. Army Electronics R & D Laboratory
Fort Monmouth, New Jersey 1

Marine Corps Liaison Officer
U. S. Army Electronics R & D Laboratory
Attn: SELRA/LNR
Fort Monmouth, New Jersey 1

Commanding Officer
U. S. Army Electronics R & D Laboratory
Attn: Director of Research
Fort Monmouth, New Jersey 1

Commanding Officer
U. S. Army Electronics R & D Laboratory
Attn: Technical Documents Center
Fort Monmouth, New Jersey 1

Commanding Officer
U. S. Army Electronics R & D Laboratory
Attn: Technical Information Division
(FOR RETRANSMITTAL TO ACCREDITED BRITISH
AND CANADIAN GOVERNMENT REPRESENTATIVES)
Fort Monmouth, New Jersey 3

Commanding Officer
U. S. Army Electronics R & D Laboratory
Attn: SELRA/PR (1 cy) (Contracts)
SELRA/PR (Mr. Hanley) (1 cy)
SELRA/PRG (Mr. Zinn) (1 cy)
SELRA/PRM (Mr. Hersh) (1 cy)
Fort Monmouth, New Jersey 4

Commanding Officer U. S. Army Electronics R & D Laboratory Attn: Logistics Division (For: SELRA/PRT Project Engineer) Fort Monmouth, New Jersey	2
Commanding Officer U. S. Army Electronics R & D Laboratory Attn: SELRA/PRT, Record File Copy Fort Monmouth, New Jersey	1
<u>Commanding General</u> U. S. Army Materiel Command Attn: R & D Directorate Washington 25, D. C.	1
Commanding General U. S. Army Combat Developments Command Attn: CDCMR-E Fort Belvoir, Virginia	1
Commanding Officer U. S. Army Communication & Electronics Combat Development Agency Fort Huachuca, Arizona	1
Hq., Electronic Systems Division Attn: ESAT L. G. Hanscom Field Bedford, Massachusetts	1
Director, Fort Monmouth Office U. S. Army Communication & Electronics Combat Development Agency Fort Monmouth, New Jersey	1
AFSC Scientific/Technical Liaison Office U. S. Army Electronics R & D Laboratory Fort Monmouth, New Jersey	1
Stanford University Microwave Laboratory, W. W. Hansen Labs Stanford, California Attn: Prof. S. Sonkin	1

Commanding Officer U. S. Army Electronics Materiel Agency 225 So. 18th Street Philadelphia, Pennsylvania Attn: SELMA-R2A	1
Director of Defense Research and Engineering Office of Secretary of Defense Washington 25, D. C. Attn: Mr. James M. Bridges	1
Advanced Research Projects Agency Office of Secretary of Defense Washington 25, D. C. Attn: Program Manager, AO 318	3
Chief, Bureau of Ships Department of the Navy Washington 25, D. C. Attn: Code 680	1
Attn: Code 335	1
Attn: Code 670B	1
Attn: Code 261B	1
Chief of Naval Operations Department of the Navy Washington 25, D. C. Attn: OP-07	1
Chief, Bureau of Naval Weapons Department of the Navy Washington 25, D.C. Attn: RRRE	1
Attn: RAAV-4423	1
Attn: RREN-3	1
Attn: RNWC	1
Applied Physics Laboratory Attn: Mr. William Dobbins Howard County, Maryland VIA: Bureau of Naval Weapons Representative Silver Spring, Maryland	1

Page 6

No. of Copies

Chief of Naval Research
Department of the Navy
Washington 25, D. C.
Attn: 461 1
Attn: 427 1

Director
U. S. Naval Research Laboratory
Washington 25, D. C.
Attn: Dr. S. T. Snith, Code 5240 1
Attn: Mr. R. C. Guthrie, Code 5300 1

Commander
New York Naval Shipyard
Naval Material Laboratory
Brooklyn 1, New York
Attn: Code 920 1

Commander, Air Force Systems Command
R & T Division
Attn: Mr. S. Tepper, RTHC
Bolling AFB, Washington 25, D. C. 1

Commander
Aerospace Systems Division
Attn: ASRNET
Wright-Patterson AFB, Ohio 1

Commander, Electronic Systems Division
Air Force Systems Command
Attn: ESRDE
Bedford, Massachusetts 1

Commander, Rome Air Development Center
Griffiss Air Force Base, New York
Attn: RCLTT 1
Attn: RCLS 1
Attn: RCLC 1
Attn: RCLTM 1
Attn: RALTP 1

Commander, Air Force Ballistic Missile Division
Air Force Unit Post Office
Attn: WZRS
Los Angeles 45, California 1

Army Missile Command Liaison Officer
Bell Telephone Laboratories
Attn: Lt. Col. Lee G. Jones
Whippany, New Jersey 1

Commanding Officer
U. S. Army Electronics R & D Laboratory
Fort Monmouth, New Jersey

Attn: SELRA/SR (Dir., Radar Div) 1
Attn: SELRA/S (Dir., Cm Div) 1
Attn: SELRA/PE (Dir., EP&M Div) 1
Attn: SELRA/N (Dir., Comm Dept) 1
Attn: SELRA/SC 1
Attn: SELRA/PEM 1

Commander
U. S. Army Materiel Command
Washington 25, D. C.
Attn: AMCRD-RS-PE-E 1

Commanding Officer
Frankford Arsenal
Attn: ORDBA-FEL
Philadelphia 37, Pennsylvania 1

Commander
Army Missile Command
Attn: ORDXM-RMP
Redstone Arsenal, Alabama 1

General Electric Company, Power Tube Department
1 River Road
Schenectady, New York
Attn: Mr. E. D. McArthur, Knolls Research Lab 1

Page 8

No. of Copies

Eitel-McCullough, Inc. 301 Industrial Way San Carlos, California Attn: Dr. George Caryotakis Attn: Mr. Earl Shelton	1 1
Radio Corporation of America Lancaster, Pennsylvania Attn: Mr. E. E. Spitzer	1
David Sarnoff Research Center RCA Laboratories Princeton, New Jersey Attn: Dr. L. S. Nergaard	1
General Electric Company Traveling Wave Tube Products Section 601 California Avenue Palo Alto, California Attn: Mr. S. E. Webber	1
Kane Engineering Laboratories 845 Commercial Street Palo Alto, California Attn: Mr. John Kane	1
Sylvania Electric Products, Inc. Chief Engineer of Microwave Device Division 500 Evelyn Avenue Mountain View, California Attn: Dr. Rudy Hutter	1
Sylvania Electric Products, Inc. East 3rd Street Williamsport, Pennsylvania Attn: Dr. John Whitmore	1
Sperry Electronic Tube Division Sperry Rand Corporation Gainesville, Florida Attn: Dr. A. D. Sutherland	1

Manager Applied Research Department Electron Tube Division Westinghouse Electric Corporation P. O. Box 746 Baltimore 3, Maryland Attn: Mr. L. R. Kilgore	1
Raytheon Company Attn: Mr. William C. Brown Waltham, Massachusetts	1
Sperry Gyroscope Company Attn: Dr. V. R. Learned Great Neck, Long Island, New York	1
Varian Associates 611 Hansen Way Palo Alto, California Attn: Dr. T. Moreno Attn: Dr. A. Staprans Attn: Dr. E. W. Herold	1 1 1
S. F. D. Laboratories 800 Rahway Avenue Union, New Jersey Attn: Dr. J. Feinstein	1
Litton Industries 960 Industrial Road San Carlos, California Attn: Dr. J. F. Hull Attn: Dr. A. Prommer	1 1
Hughes Aircraft Company Culver City, California Attn: Dr. L. M. Field, Microwave Tube Division	1
Watkins-Johnson Company 3333 Hillview Avenue Palo Alto, California Attn: Dr. Rolf Peter	1

Field Emission Corporation
McMinnville, Oregon
Attn: Dr. F. M. Charbonnier 1

Sperry Gyroscope Company
Division of Sperry Rand Corporation
Great Neck, Long Island, New York
Attn: D. Churchill 1
Attn: J. McLinden 1

General Electric Company
Superpower Microwave Tube Laboratory
1 River Road
Schenectady, New York
Attn: R. Bondley, Knolls Research Laboratory 1

Eitel-McCullough, Inc.
301 Industrial Way
San Carlos, California
Attn: L. Reed 1

Stanford Research Institute
Menlo Park, California
Attn: L. Feinstein 1

General Telephone and Electronics Corporation
Bayside Laboratory
Bayside, New York
Attn: B. W. Leavitt 1

Mitronics, Inc.
132 Floral Avenue
Murray Hill, New Jersey
Attn: S. S. Cole 1

General Electric Company
3001 East Lake Road
Erie, Pennsylvania
Attn: J. J. Cacciotti 1

Page 11

No. of Copies

Ford Instrument Company
31-10 Thomas Avenue
Long Island City, New York
Attn: W. Franklin 1

Director, Lincoln Laboratory
P. O. Box 73
Lexington 73, Massachusetts
Attn: Dr. G. L. Guernsey 1

Stanford University
Microwave Laboratory
Stanford, California
Attn: Prof. M. Chodorow, Director 1

Aerospace Corporation
Los Angeles 45, California
Attn: Dr. I. Getting 1

Los Angeles Air Procurement Center
Attn: Administrative Contracting Officer
The RAND Corporation
1700 Main Street
Santa Monica, California 1

Project M
Stanford University
Stanford, California
Attn: Mr. J. Jasberg 1

Polytechnic Institute of Brooklyn
55 Johnston Street
Brooklyn 1, New York
Attn: J. W. Griemsmann 1

Physics Laboratory
University of Utah
Salt Lake City, Utah
Attn: P. Gibbs 1
Attn: G. Baker 1

Page 12

No. of Copies

Laboratory for Insulation Research
Massachusetts Institute of Technology
Cambridge, Massachusetts
Attn: D. A. Powers 1

Battelle Memorial Institute
505 King Avenue
Columbus 1, Ohio
Attn: Defender Library 1

Cornell Aeronautical Laboratory, Inc.
4455 Genesee Street
~~Buffalo 21, New York~~
Attn: Mr. R. C. Beitz 1

MITRE Corporation
Bedford, Massachusetts
Attn: Dr. R. F. Naka, Associate
Technical Director, Bldg. 2A-251 1

Chief, Army Research Office
Washington 25, D. C. 1

Hq., U. S. Air Force
Attn: AFRST-EL-CS
Rm. 4D-335 Pentagon
Washington 25, D. C. 1

USAE LRDL Liaison Office
Rome Air Development Center
ATTN: RAOL
Griffiss Air Force Base, New York 1

Director, R & D
Army Materiel Command
Attn: Development Division
Temporary Bldg. T, Gravelly Point
Washington 25, D. C. 1

Commander European Office of Aerospace Research Attn: Lt. Col. O. R. Hill, The Shell Bldg. 47 Rue Cantersteen Brussels, Belgium	1
Bell Telephone Laboratories, Inc. Whippany, New Jersey Attn: Mr. R. C. Newhouse	1
RCA Aerospace Communication and Controls Division P. O. Box 588 Burlington, Massachusetts Attn: Mr. W. Ramsey	1
Jet Propulsion Laboratory California Institute of Technology 4800 Oak Grove Drive Pasadena, California Attn: 05.00/31, Mr. I. E. Newlan, Mgr. Tech. Reports Section	1
Microwave Associates, Inc. Burlington, Massachusetts Attn: Dr. Grant St. John	1

<p>Eitel-McCullough, Inc., San Carlos, California</p> <p>Microwave Window Multipactor and Its Inhibition, by O. Heil and D. Preist</p> <p>Quarterly Progress Report No. 2, December 1962, 66 pages including illustrations</p> <p>Contract DA-36-039 SC-90818, DA Task No. OST-76-10-318-28-03, Unclassified Report</p> <p>The test results of this period are discussed. Uncoated alumina and beryllia windows were tested under CW conditions to determine power level at multi-</p> <p>(over)</p>	<ol style="list-style-type: none"> 1. Multipactor 2. Microwave Windows 3. Microwave Power Generation 4. Microwave Tubes 5. Dielectric <p>I. Heil, Oskar</p> <p>II. Preist, Donald</p> <p>III. Project Defender</p> <p>IV. USAELRDL Contract No. DA-36-039 SC-90818</p> <p>V. DA Task No. OST-76-10-318-28-03</p> <p>VI. In ASTIA Collection</p>	<p>Eitel-McCullough, Inc., San Carlos, California</p> <p>Microwave Window Multipactor and Its Inhibition, by O. Heil and D. Preist</p> <p>Quarterly Progress Report No. 2, December 1962, 66 pages including illustrations</p> <p>Contract DA-36-039 SC-90818, DA Task No. OST-76-318-28-03, Unclassified Report</p> <p>The test results of this period are discussed. Uncoated alumina and beryllia windows were tested under CW conditions to determine power level at multi-</p> <p>(over)</p>	<ol style="list-style-type: none"> 1. Multipactor 2. Microwave Windows 3. Microwave Power Generation 4. Microwave Tubes 5. Dielectric <p>I. Heil, Oskar</p> <p>II. Preist, Donald</p> <p>III. Project Defender</p> <p>IV. USAELRDL Contract No. DA-36-039 SC-90818</p> <p>V. DA Task No. OST-76-10-318-28-03</p> <p>VI. In ASTIA Collection</p>
<p>pector initiation and the effects of crossed magnetic fields on multipactor. Coating techniques are described. Results of nine coated and uncoated, grooved and ungrooved alumina and fused silica windows evaluated in a pulsed ring resonator are discussed. Mathematical analyses of electron motion under single surface multipactor, and of the effects of radiation pressure on electron motion are provided.</p>		<p>pector initiation and the effects of crossed magnetic fields on multipactor. Coating techniques are described. Results of nine coated and uncoated, grooved and ungrooved alumina and fused silica windows evaluated in a pulsed ring resonator are discussed. Mathematical analyses of electron motion under single surface multipactor, and of the effects of radiation pressure on electron motion are provided.</p>	